NASA Contractor Report 174796

Analysis Techniques for Tracer Studies of Oxidation

Soumendra Nath Basu

Case Western Reserve University
Cleveland, Ohio

November 1984

TABLE OF CONTENTS

iii

CHAPTER 1

INTRODUCTION

The double oxidation technique using O-18 as a tracer has been successfully used to identify the transport mechanisms in growing oxide scales. The detailed mechanism of oxidation is of more than academic interest as it determines growth stresses and oxide spallation. The aim of this study was to develop analysis techniques to obtain quantitative diffusion data from the tracer concentration profiles in growing oxide scales. An oxide can grow inward at the metal-oxide interface by inward oxygen diffusion, it can grow outward at the gas oxide interface by outward cation diffusion or it can grow by a combination of both the mechanisms. The problem of determining the fraction of inward and outward growth of the scale from the tracer concentration profile was solved. The process of tracer diffusion in a growing polycrystalline scale was theoretically modelled.

The analysis techniques developed were then applied to a FeCrAl-Zr alloy by using SIMS to obtain the tracer profile.

CHAPTER 2

LITERATURE SURVEY

2.1 Mathematics of diffusion

2.1.1 Diffusion

Atoms in a solid are in constant motion about their lattice sites. Occasionally, a few atoms gain sufficient energy to jump into neighbouring sites. This random movement of atoms is called diffusion. Self diffusion is the phenomenon of migration of atoms in the absence of concentration gradients. Self diffusion can be studied by introducing an isotopic tracer into the system such that the diffusing atoms can be identified. Strictly speaking the diffusion coefficients of isotopes are related by the equation:

$$\frac{D_2}{D_1} = \left(\frac{M_2}{M_1}\right)^{1/2} \qquad \ldots(2.1)$$

Where M_1 and M_2 are the masses and D_1 and D_2 are the diffusion coefficients of the isotopes. However, generally the isotopic masses are so close to each other that the diffusion coefficients are assumed to be the same. When O-18 is used as a tracer to study oxygen diffusion, the difference

3

is about 6%.

2.1.2 Fick's laws

Matter flows in a manner to decrease its concentration gradient or more precisely its chemical potential gradient. The flux density, J_i (kg/m^2 sec), of the species i in 3 dimensions is given by:

$$J_i = -D_i \, \rho \, \nabla C_i \qquad \ldots(2.2)$$

Where D is the diffusion coefficient (m^2/sec), ρ is the density (kg/m^3) and C_i is the mass fractional concentration gradient (m^{-1}). This is Fick's first law. In 1-dimension Equation 2.2 becomes:

$$J_i = -D_i \, \rho \, \frac{\partial C_i}{\partial x} \qquad \ldots(2.3)$$

From Equation 2.3 and using the principle of mass conservation [1] it can be shown that:

$$\frac{\partial C_i}{\partial t} = \frac{\partial}{\partial x}\left(D_i \, \frac{\partial C_i}{\partial x}\right) \qquad \ldots(2.4)$$

where t is the time. This is Fick's second law. If D_i is independent of position , Equation 2.4 becomes:

$$\frac{\partial C_i}{\partial t} = D_i \, \frac{\partial C_i}{\partial x^2} \qquad \ldots(2.5)$$

2.1.3 Diffusion mechanisms

Diffusion generally occurs by a vacancy or an interstitial mechanism. An atom adjacent to a vacancy can exchange sites with the vacancy and thus migrate through the crystal. Some atoms occupy positions in the interstices of the crystal lattice. They can move either by jumping from an interstitial site to another (interstitial mechanism) or by displacing a lattice atom into an interstitial position and taking up the lattice site itself (interstitialcy mechanism).

The predominant point defects in an ionic crystal are [2]:

i) Schottky disorder- Stoichiometric proportion of cations and anion vacancies.

ii) Frenkel disorder- Equal number of cation vacancies and interstitials.

iii) Anti Frenkel disorder- Equal number of anion interstitials and vacancies.

iv) Anti Schottky disorder- Stoichiometric proportion of anion and cation interstitials.

5

It should be noted that the experimental diffusion coefficient can be represented by an Arrhenius type equation:

$$D = D_o \exp \left(-\frac{Q}{RT}\right) \qquad \ldots(2.6)$$

where D_o is the preexponential term (m^2/sec) and Q is the activation energy (kJ/mole).

2.2 Grain boundary diffusion

2.2.1. Introduction

Enhanced grain boundary diffusion has been observed in several oxides [3-4]. The observed tracer concentration profile in a polycrystalline sample is due to both fast diffusion along the grain boundaries and slower diffuson into the grains from the surface and the grain boundaries. Some of the models proposed to mathematically treat the combined grain boundary and volume diffusion problem are discussed in the next section.

2.2.2 Mathematical treatment

Fisher [5] modelled a grain boundary as a thin slab of thickness ω extending into a semi infinite crystal (Figure 1) The diffusion coefficient D_b in the grain boundary is much greater than the diffusion coefficient in the crystal. Whipple [6] used the Fisher model and obtained exact solutions of the average tracer concentration profile using Fourier - Laplace transforms. He used a constant source condition i.e.,

$$C(x,y,t)=C_o \quad \text{for } t>0 \text{ and } y=0$$

He obtained that the logarithm of the average tracer concentration $(\ln \overline{C})$ varies linearly with $y^{6/5}$ with a slope that can be related to the grain boundary diffusion coefficient by the equation :

$$D_b \omega = \left(\frac{\ln \overline{C}}{y^{6/5}} \right) \left(\frac{4D}{t} \right) \left(\frac{\ln \overline{C}}{(\eta \beta^{-1/2})^{6/5}} \right)^{5/3} \quad \ldots(2.7)$$

where:

$$\eta = \frac{y}{\sqrt{Dt}} \quad , \qquad \beta = \frac{(\Delta-1)\omega}{\sqrt{Dt} \, 2} \qquad \Delta = \frac{D_b}{D}$$

Levine and MacCallum [7] solved the grain boundary diffusion equation directly for the average concentration in polycrystalline samples
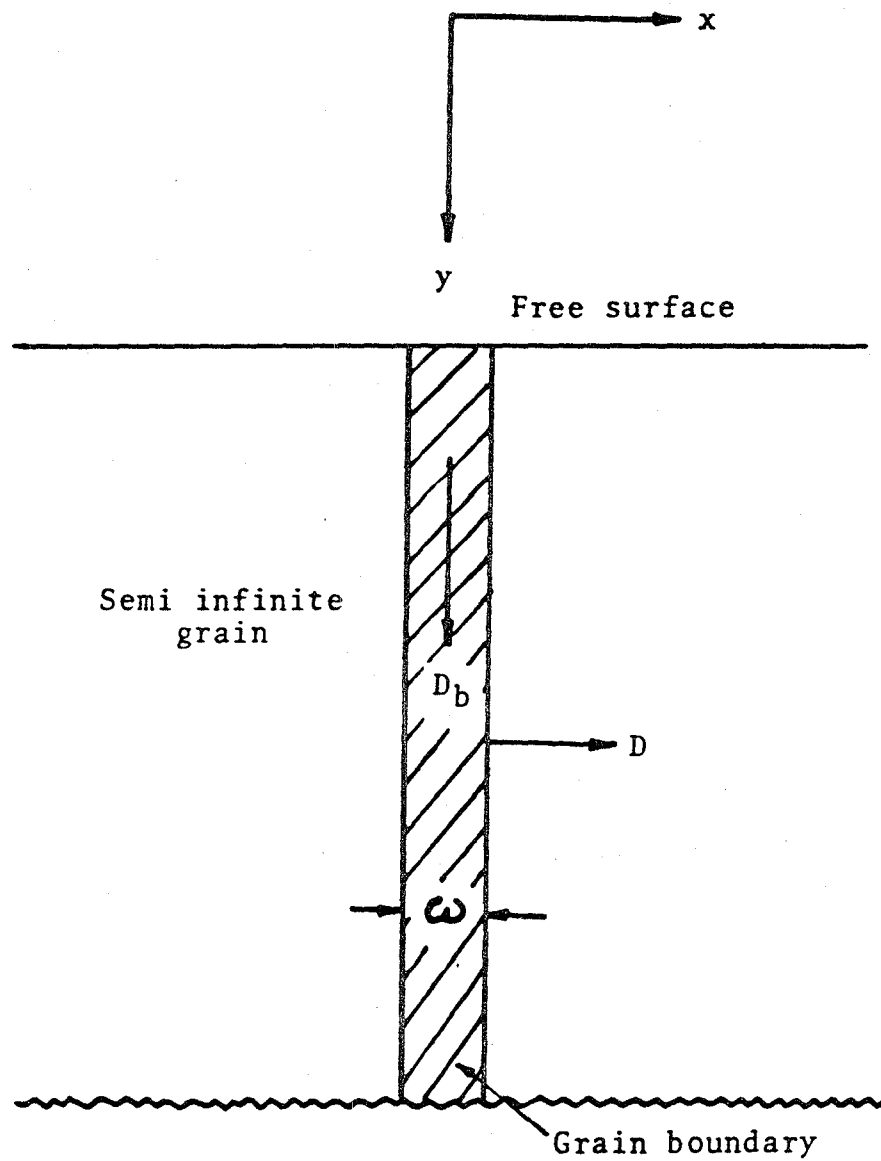
FIGURE 1 - Fisher's model of a grain boundary.

and found that for $\beta > 10$ the last term in Equation 2.7 is independent of $\eta\beta^{-1/2}$ and is equal to 0.78. This was later confirmed for Whipple's solution by LeClaire [8].

Suzuoka [9] solved the same problem, but assumed an instantaneous source condition ie.,

$$C(x,y,t)=K \ \delta(y) \qquad x=0, \ t=0$$

where K is the surface density of the planer source. His solution also predicted a linear plot between $\ln \bar{C}$ and $y^{6/5}$ with:

$$\frac{\partial \ln \bar{C}}{\partial (\eta\beta^{-1/2})^{6/5}} = 0.75$$

Thus to obtain the value of $D_b\omega$, experimental values of $\ln \bar{C}$ can be plotted against $y^{6/5}$. A straight line can be fitted to the data points of deeper penetrations. The slope of this line can be used to determine the value of $D_b\omega$ using Equation 2.7.

Zaeschmar [10] treated the grain boundary diffusion problem by considering the polycrystal as a 3-dimensional brickwork of cylindrical grains. He introduced another empirical parameter - the filling time of a grain. Oishi and Ichimura [11] treated the problem as the homogeneous filling of a grain pinned to the grain boundary

9

at an arbitrary distance from the surface. As this
author has used the Oishi-Ichimura geometrical
configuration for modelling, it will be described
in detail later.

2.3 Previous studies of oxygen diffusion in
    alumina

2.3.1. Lattice diffusivity

Oishi and Kingery [12] studied oxygen
diffusion in single crystal alumina using gaseous
exchange technique. Their plot of log (D) versus
1/T showed a break at 1650 $^\circ$C which was interpreted
as an extrinsic to intrinsic transition. The high
temperature data showed that:

$$D = 1.9 \times 10^{-1} \exp(\frac{-636 \text{ kJ/mole}}{RT}) \text{ m}^2/\text{sec} \quad ...(2.8)$$

while the fit to the low temperature data
suggested that:

$$D = 6.3 \times 10^{-12} \exp(\frac{-241 \text{ kJ/mole}}{RT}) \text{ m}^2/\text{sec} \quad ...(2.9)$$

This was later shown to be an experimental artifact
sensitive to the surface preparation of the
specimen. When the samples in the low temperature
region were preannealed before the diffusion
anneal, the measured diffusion coefficients fell
on the extrapolation of the high temperature data.

10

Oishi, Ando and Matsuhiro [13] studied high purity vapour grown crystals using the same method as Oishi and Kingery. Their results were in approximate agreement with Oishi and Kingery's results.

Reed and Weunsch [14] studied single crystal alumina using ion probe. Their data suggest that:

$$D = 6.4 \exp(\frac{-787 \ kJ/mole}{RT}) \ m^2/sec \ ...(2.10)$$

Reddy and Cooper [15] exchanged single crystal alumina in enriched O-18 gas and measured the tracer concentration profile using proton activation. Their data fit the equation:

$$D = 2.66 \times 10^{-2} \exp(\frac{-615 \ kJ/mole}{RT}) \ m^2/sec \ ...(2.11)$$

Cawley, Halloran and Cooper [16] exchanged single crystal alumina in Reddy's gas exchange apparatus. The tracer profiles were determined by both proton activaton and Secondary Ion Mass Spectrometry (SIMS). Cawley found that the diffusion coefficient of oxygen was insensitive to impurity levels and oxygen partial pressure and could be described by:

$$D = 1.51 \times 10^{-3} \exp(\frac{-527 \ kJ/mole}{RT}) \ m^2/sec \ ...(2.12)$$

Recently Laserlof, Heuer and Mitchell studied the annhilation of dislocation loops by annealing deformed cylinders of Al_2O_3. Based on the assumption that the self diffusion of oxygen was rate controlling they calculated the diffusion coefficient of oxygen in undoped alumina as:

$$D = 6.8 \times 10^{-4} \exp(\frac{-587 \text{ kJ/mole}}{RT}) \text{ m}^2/\text{sec} \quad ...(2.13)$$

It should be noted that the data of Oishi and Ando, Reddy and Cooper, Cawley, Halloran and Cooper, and Laserlof and Heuer, taken by using different techniques, agree well in the temperature range of 1250 to 1800 ^{o}C. So the lattice diffusion coefficient of oxygen in pure alumina is well established.

2.3.2 Grain boundary diffusivity

Mistler and Coble [17] calculated grain boundary diffusion coefficients and widths from the results of grain growth, creep, sintering and diffusion. Mathematical models of sinterns and creep gave $D_b \omega$ while grain growth models were assumed to give D_b / ω. Thus D_b and ω were calculated separately. The grain boundary width for alumina was reported to be between 9-12 nm

while the grain boundary diffusion coefficient was reported as:

$$D_b = 5.15 \times 10^{-4} \exp(\frac{-451 \text{ kJ/mole}}{RT}) \text{ m}^2/\text{sec} \quad ...(2.14)$$

There is a lot of uncertianty in these results as the effect of impurities on grain growth was neglected. The model assumed an effective diffusion coefficient D_{eff} given by:

$$D_{eff} = \epsilon D_b + (1-\epsilon)D$$

where ϵ is the volume fraction of the grain boundaries. The above expression does not take into consideration the diffusion from the grain boundaries into the grains.

Johnson and Berrin [18] used initial stage sintering studies to obtain:

$$D_b \omega = 5.2 \times 10^{-4} \exp(\frac{-653 \text{ kJ/mole}}{RT}) \text{ m}^3/\text{sec} \quad ...(2.15)$$

However their model neglected the contribution of surface diffusion to the neck growth.

Lessing and Gordon [19] used creep results of iron doped alumina samples to obtain:

$$D_b \omega = 4.38 \times 10^{-7} \exp(\frac{-439 \text{ kJ/mole}}{RT}) \text{ m}^3/\text{sec} \quad ...(2.16)$$

However they had to guess the rate controlling diffusion process. At large concentrations of divalent iron and large grain size the creep was

assumed to be limited by oxygen grain boundary
diffusion.

Reddy and Cooper [15] used proton activation
on undoped polycrystalline alumina to obtain:

$$D_b = 4.41 \times 10^{-3} \exp(\frac{-690 \text{ kJ/mole}}{RT}) \text{ m}^2/\text{sec} \ldots (2.17)$$

The boundary widths assumed were typically 15 to
40 nm. This assumption is too large as the grain
boundary width of alumina is typically closer to
10Å[*]. There is thus a great degree of disagreement
between the reported values of grain boundary
diffusivity and boundary width.

2.4 Oxidation of superalloys

2.4.1 Superalloys

The need to develop materials for high
temperature applications like gas turbine engines
led to the development of superalloys [20]. MCrAl
alloys (M=Fe,Ni,Co) are promising for use upto
1200°C. The high strength of these alloys is
achieved by solid solution and precipitation
hardening while good oxidation resistance is
obtained by the formation of adherent protective
oxide layers. These alloys owe their oxidation
----
* Personal communications with N.L.Peterson of
  Argonne National Laboratories.

14

resistance to the formation of an alumina scale since it is the most stable oxide and has the lowest free energy of formation. Alumina is a stoichiometric oxide with low diffusion rates and is not attacked by either H_2O or CO_2. Giggins and Pettit [21] showed that the external alumina scale forms for certain compositions of the alloy only. The amount of aluminum needed to form a continuous scale can be reduced by increasing the chromium content as chromium acts as an oxygen getter.

2.4.2. Transient scales

Though the superalloys owe their oxidation resistance to the formation of a protective alumina scale, it has been found that initially transient oxides are formed., Smialek and Gibala [22] studied the structure of transient scales formed on pure, Y doped and Zr doped NiCrAl alloys. Oxidation of these alloys for 0.1 hour at $1100^{\circ}C$ produced oriented $\gamma - Al_2O_3$, $\alpha - (Al,Cr)_2O_3$ or a spinel like $Ni(Cr,Al)_2O_4$ before the random $\alpha-Al_2O_3$ layer was formed. The scales were densely populated with internal precipitates and there was evidence of plastic flow in the underlying metal due to growth

15

stresses. The formation of coherent layers of aluminium depleted phases indicated the selective removal of aluminium at these short times.

Golightly, Wood and Stott[23] studied the oxidation of FeCrAl alloys with various Y additions at 1100°C and 1200°C. They observed the formation of transient oxides rich in iron and chromium in all cases which was followed by the steady state α-alumina scale. For the Y free alloy it was found that the steady state was reached faster if the chromium content or the temperature was increased. The amount of transient oxide formed was also determined by the specimen surface topography since the development of the α-alumina layer was less rapid at the base of the alloy asperities than at a flat alloy oxide interface.

2.4.3 Mechanism Of Oxidation

Inert marker experiments by Hindam and Smeltzer [24] indicated that alumina scales grow inward by oxygen diffusion. Recent O-18 tracer studies by Reddy [25] have also confirmed that the

16

Primary transport is oxygen inward and the profiles are most consistent with the grain boundary transport model.

Golightly et al. [26] observed that the growth morphology of alumina scales on FeCrAl alloys was different for Y free and Y containing alloys. They suggested that in the Y free alloy, the scale grew by a combined inward oxygen and outward aluminum transport mechanism which caused lateral growth within the scale. This was responsible for the highly stressed oxide on the Y free alloys. The absence of growth stresses and lateral growth in scales with Y was attributed to the blocking of outward aluminum diffusion.

Whittle and Stringer [27] proposed a nucleation model to explain the 'Rare earth effect'. They suggested that the rare earth additions acted as nucleation sites for all the oxide phases, thus producing a finer grained initial oxide. This caused the steady state oxidation to be reached more rapidly and at a lower aluminum or chromium content.

2.4.4 Oxide adherence

As discussed earlier, the introduction of small amounts of rare earth elements to the superalloys caused a dramatic improvement in the scale adherence. Some of the mechanisms put forward to explain this phenomenon are as follows [27,28]:

a) Y (or other rare earth elements) improve the chemical bond at the metal-oxide interface as they have a better affinity for oxygen than the alloying elements.

b) Yttride precipitates or yttria particles can induce mechanical pegging of the oxide scale on the substrate.

c) Y promotes the formation of an inner yttria layer which acts as a diffusion barrier and also decreases the mechanical and thermal stresses between the oxide and the alloy.

d) Soluble Y in the alloy can trap the metal vacancies and consequently avoid vacancy coalescence at the metal oxide interface.

e) Y present in the oxide scale can infuence oxide defect mobility and consequently the diffusion rate in the oxide scale, oxide thickness and plasticity.

Delaunay et al. studied the mechanical stresses generated in the oxide scale during the oxidation of superalloys. They concluded that Y improves the oxide adherence by trapping the vacancies and preventing them from precipitating at the metal oxide interface [29].It may also improve the oxide plasticity by increasing the concentration of oxygen vacancies [30].

2.4.5 Growth kinetics and microstructure of FeCrAl-Zr alloy

Smialek studied the microstructure of the oxide grown on the FeCrAl-Zr alloy used by this author. He saw monoclinic zirconia precipitates at the grain boundaries at the gas surface. There were deep depressions in the large grains at the metal-oxide interface which represented areas where the grain boundary regions had advanced faster than the interior of the grains due to

19

short circuit diffusion [31,32,33]. At 1100 ^{o}C, the growth rate of the oxide was found to obey the law:

$$X = (K_p t)^{0.46} \qquad \ldots(2.18)$$

Where X is the oxide thickness and t is the oxidation time. The grain growth in the alumina scale was found to obey the law:

$$Grain\ size = (K_s t)^{0.2} \qquad \ldots(2.19)$$

There was a variation of grain size and shape across the scale. The grains near the gas surface were spherical and small in size while the grains near the oxide-metal interface were larger in size and columnar in shape.

2.5. Previous O-18 sudies

O-18 has been successfully used as a tracer to identify the growth mechanisms of oxide scales. The double oxidation technique consists of successive oxidation of the alloy in natural oxygen and O-18 tracer. The concentration profile of the tracer is determined by some convenient technique like proton activation or SIMS. The tracer can then be used to identify the regions of new growth. The shape of the tracer concentration

20

profile can provide insight into the mechanism of oxide growth.

O-18 has been succesfully used as a tracer by many workers. Lees and Calvert [34] used the double oxidation technique on FeCr alloys in 1976. In 1978, Sheasby and Brown[35] used SIMS to obtain O-18 concentration profiles in CoO scales. In 1980, Hartley et al. [36] at Harwell oxidized FeCr alloys in a $C^{18}O_2$ atmosphere. They used proton activation to obtain the tracer concentration profiles. In 1982 Lees et al. studied the mechanism of corrosion of low silicon [37] and high silicon [38] ferritic steels in high pressure CO_2 using O-18 tracer.

Reddy[15] used the double oxidation technique to measure oxygen diffusivities in various oxides. He used the proton activation technique to measure the tracer concentration profiles. Reddy also studied the oxidation mechanism of NiCrAl alloys by the double oxidation technique. Very recently Cawley studied the self diffusion coefficient of oxygen in alumina using O-18 tracer. He determined the tracer profiles by both proton

activation and SIMS. Cawley also studied the thermal oxidation of silica and silicon carbide using the same technique. He was able to obtain good fits of his data to the theoratical calculations if he assumed different diffusion coefficients for his near surface and deep profiles.

2.6. SIMS

In SIMS [39],the sample is bombarded with high energy primary ions (Ar^+ in this case). These primary ions penetrate into the solid where binary collisions with target atoms occur. The primary atoms come to rest at the so called penetration depth and are thus implanted in the solid. These primary ions cause the target atoms to be displaced from the surface due to various generation target recoils. These target or secondary ions are passed through a mass analyzer where they are separated by mass to charge ratios. An electron beam is also focussed on the sample to keep it neutral.

The number of sputtered secondary ions of a given type is a complex function of the surface concentration, electronic structure and sputtering conditions. However, as all the variables for isotopes are almost the same, the ratio of counts of isotopic ions gives the true value of isotopic concentration.

The resolution of SIMS is limited by non-uniform sputter etching which may yield sputtered species from a range of depths [40,41]. This problem is particularly severe at the edge of the crater. To avoid this problem the raster gating technique is used where the beam scans over a large area and detects secondary ions from the central portion of the crater only. Another problem faced when sputtering insulators is that of charging due to ion removal. If the charging is stable it can attenuate the secondary ion signal [42]. The electron beam can neutralize the secondary ions, causing further complications.

The advantage of using SIMS over proton activation is its depth resolution which is less than 10$\overset{o}{A}$. Also there is no limit on the depth of the sputtered crater exept for the machine time. SIMS also provides the data in a very convenient form and can monitor upto 9 elements at a time.

However, the problems of non uniform sputtering, especially in polycrystalline samples can severely limit the resolution of SIMS and can actually make the data worthless. This point will be discussed in detail later. The conversion of counts to concentration with the help of standards can be extremely unreliable as the ion yield depends on, among other things, the sample surface preparation, the incident angles of the ions and the sample microstructure. So it is extremely important to apply stringent tests on the quality of data before any quantitative information is obtained from it.

CHAPTER 3

THEORY

3.1 Statement of the Problem

O-18 has been successfully used as a tracer to
identify the growth mechanisms in oxide scales.
The double oxidation technique is used to identify
the diffusion processes involved. In this
technique the alloy is sequentially oxidized, first
in natural oxygen and then in O-18 tracer. The
oxide grown during the natural oxygen oxidation is
referred to as the old oxide while the oxide grown
during the tracer oxidation is referred to as the
new oxide. The position of the new oxide growth is
determined from the concentration profile of the
tracer across the oxide scale. The tracer
concentration profile is obtained by SIMS.

It has been shown that the primary transport
mechanism operative during the growth of α-alumina
scales on superalloys is inward grain boundary
diffusion of oxygen [15,32] .Thus the protective
oxide scale has been found to be primarily inward

25

growing. However, as the oxygen tracer diffuses down the grain boundaries, it exchanges with O-16 existing in the grains. To get any quantitative information from the tracer concentration profile, it is necessary to model this process of inward tracer grain boundary diffusion with exchange. The advantage of a quantitative model is that the grain boundary and the lattice diffusion coefficients can be obtained from the shape of the tracer concentration profile. The effect of structural parameters like the oxide grain size on the tracer profile can also be studied. It can also be used to determine if the scale is inward or outward growing. In the case where scale growth is a combination of both the mechanisms, a simple mass balance test can be used to separate the two processes. To model the diffusion process, Oishi and Ichimura's geometrical configuraton of the grain boundaries and grains have been used.

In the model, the shape of the tracer concentration profile depends on the three parameters:

1) the grain size r, 2) the grain boundary

26

diffusion coefficient D_b and 3) the lattice diffusion coefficient D. By choosing the appropriate values of the three parameters, a family of curves can be generated which define a range of O-18 profiles which are quantitatively compatible with the inward oxygen diffusion mechanism. Conversely, given an experimental tracer concentration profile, it should be possible to pin down the values of the three parameters. It should be noted that the grain size of the oxide scale can be obtained by SEM studies. A good estimate of the grain boundary diffusion coefficient can be obtained from the growth kinetics of the oxide while values of the lattice diffusion coefficient can be obtained from the literature. Thus there is independent information existing for all the three model parameters. A major assumpton made during the modelling of the diffusion process is that the oxide scale grows in a planar fashion.
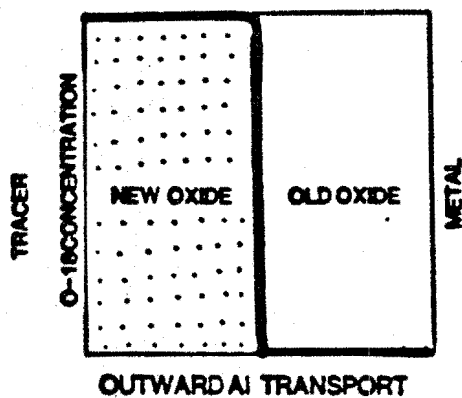
3.2 Expected Tracer Profiles

27

Figure 2 shows the schematic O-18 concentration profiles for various transport mechanisms. If the outward aluminum transport is the primary mechanism the scale will be outward growing. The tracer concentraton profile will be a step function due to the formation of $Al_2^{18}O_3$ at the gas-oxide interface. If the transport mechanism is inward oxygen grain boundary transport, the scale will be inward growing and the concentration profile will be a step function due to the formaton of $Al_2^{18}O_3$ at the metal-oxide interface. This is however an ideal case. When the tracer in the grain boundaries comes in contact with O-16 in the grains of the old scale, exchange will take place and the concentration profile will look like Figure 2c). Finally if the diffusion mechanism is a combination of outward aluminium and inward oxygen transport the tracer profle would look like Figure 2d).
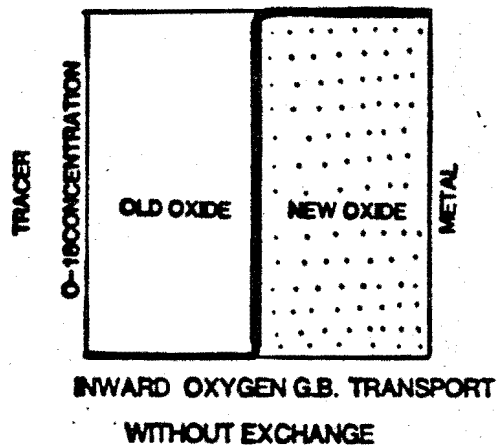
3.3 Mass Balance

Given a tracer concentration profile across the oxide scale a simple mass balance test can be used to determine the growth mechanism. As shown
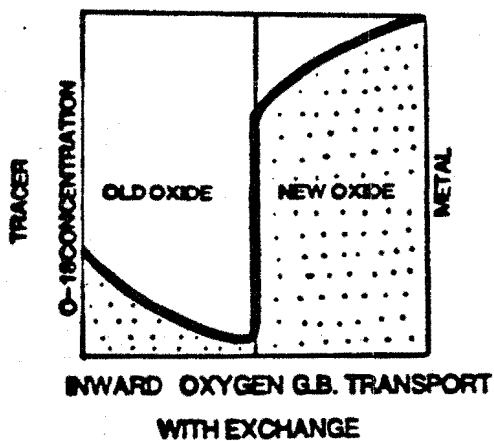
28

OUTWARD AI TRANSPORT

a)

INWARD OXYGEN G.B. TRANSPORT

WITHOUT EXCHANGE

b)

INWARD OXYGEN G.B. TRANSPORT

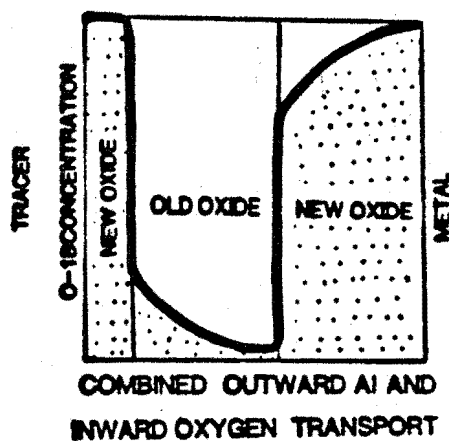WITH EXCHANGE

c)

COMBINED OUTWARD AI AND

INWARD OXYGEN TRANSPORT

d)

FIGURE 2 - Schematic tracer concentration profiles
for various transport mechanisms.

in Figure 3, a normalized concentration profile can
be plotted such that the X-axis is a plot of the
fraction of the total scale thickness while the
Y-axis is the plot of the concentration of the
tracer as a fraction of the maximum tracer
concentration in the scale.

We know that every atom of O-18 in the
oxide scale got there when the sample was exposed
to the tracer. Thus the number of lattice sites
occupied by the tracer atoms in the oxide scale
must be the same as the number of oxygen lattice
sites created in the oxide during the tracer
oxidation. This concept can be used to calculate
the thickness of the new oxide Y_{new} as shown in
Figure 3b). Y_{new} is so chosen, that area A in
Figure 3a) (amount of O-18 in the total oxide) is
equal to the area B in Figure 3b) (amount of oxygen
in the new oxide). Having established the new
oxide thickness, it can be determined if the growth
mechanism is primarily inward oxygen transport or a
combinaton of outward aluminum and inward oxygen
transport. If the diffusion mechanism is inward
transport of oxygen through the grain boundaries
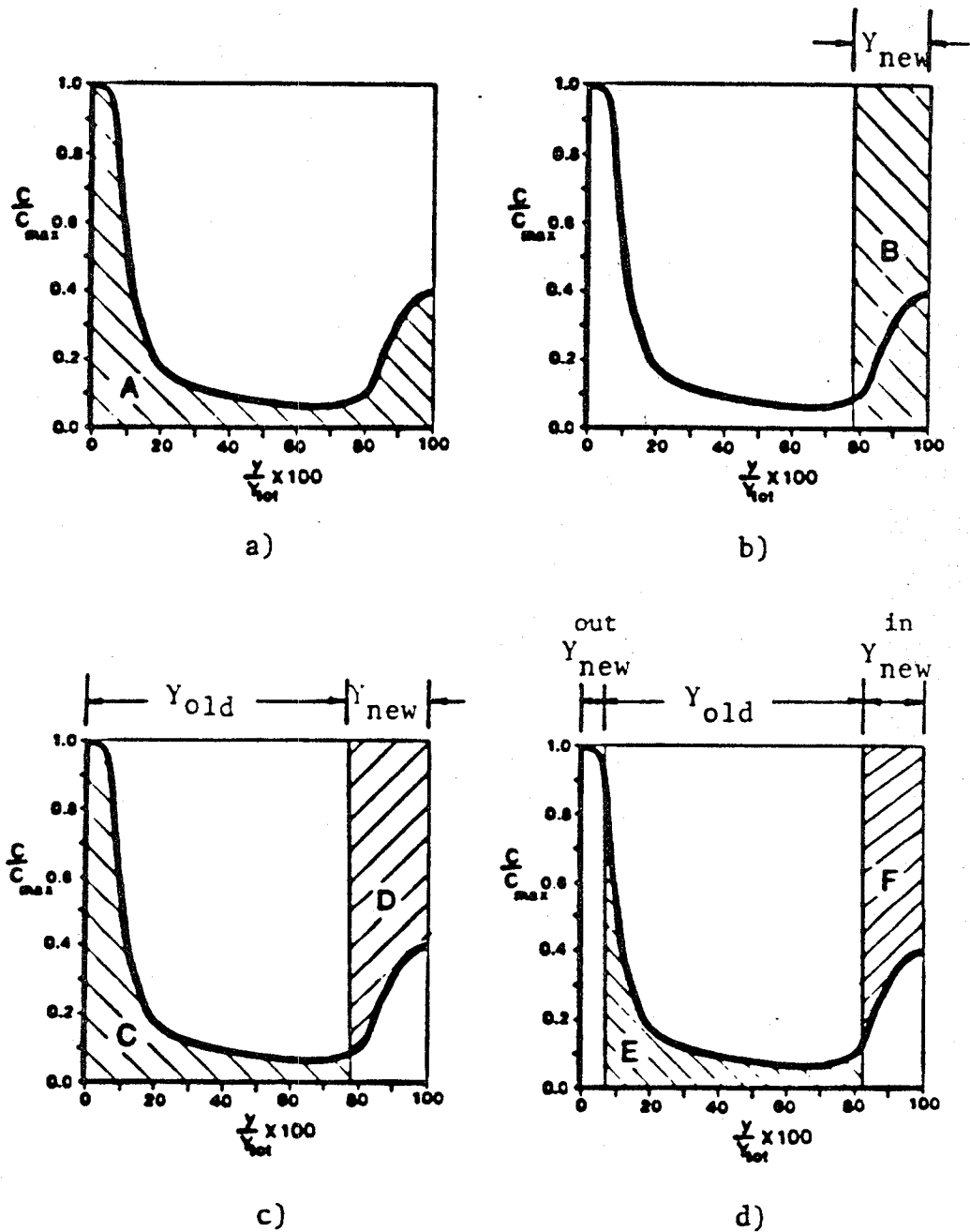with exchange, the scale is inward growing. Then

FIGURE 3 - Determination of transport mechanisms by
mass balance.

the number of O-18 atoms retained in the old oxide

must be the same as the number of O-16 atoms found

in the new oxide as they are both involved in the

same exchange process. Thus if area C is equal to

the area D in Figure 3c) the transport mechanism is

inward oxygen diffusion. However, if area C is

greater than area D some of the tracer atoms in C

did not get there due to exchange but rather due to

outward aluminium diffusion leading to the

formation of $Al_2O_3^{18}$ at the gas-oxide interface. In

this case, it is possible to determine, at least in

principle, what fraction of the scale growth is due

to each mechanism. Thus Y_{new} can be split up into

Y_{new}^{in} and Y_{new}^{out} such that area E=area F in Figure 3d).

This allows the growth kinetics to be split up into

inward growth and outward growth and both these can

be separately analysed. So with profiles of

sufficient quality, one can obtain detailed

information by simple mass balance analysis. It

should be noted that this is model free.

It should be mentioned that the mass balance

criterion is valid if the number of tracer atoms in

the grains at the oxide-gas interface due to direct

surface exchange with the gas is neglected. This

is a valid assumption because the grain boundary
diffusivity is much higher than the lattice
diffusivity in the oxide and the penetration depth
of the tracer atoms due to volume diffusion at the
surface is neglisible.

Much more informaton can be obtained from the
actual shape of the tracer concentration profile,
if the actual equations describing tracer
incorporation during scale growth could be directly
solved. Even in the simple case of inward oxygen
diffusion it is a formidable problem of combined
lattice and grain boundary diffusion with a moving
boundary under an imposed field. However a
relatively simple but still realistic model permits
the diffusion equations to be solved.

3.4 Geometrical Configuration

Figure 4 shows an idealised drawing of the old
scale with hexagonal grains arranged in a close
packed two dimensional network. These grains are
formed during the O-16 oxidation and contain
natural oxygen atoms. When the sample is exposed
to the tracer, O-18 diffuses rapidly down the grain

O-18 GAS

TRACER DIFFUSING
THROUGH GRAIN
BOUNDARIES

TRACER EXCHANGE
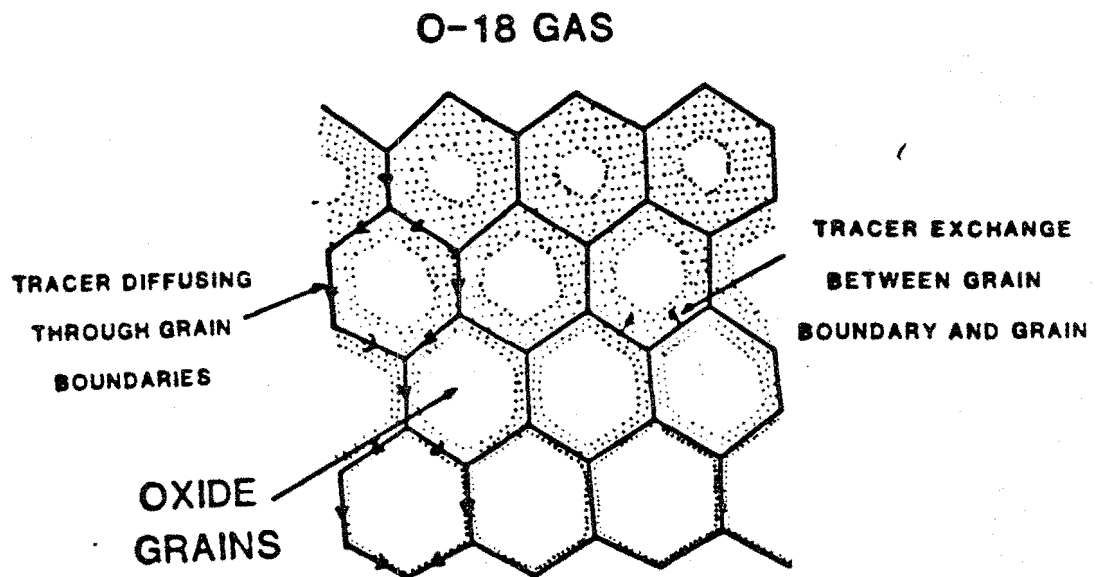BETWEEN GRAIN
BOUNDARY AND GRAIN

OXIDE
GRAINS

FIGURE 4 - Schematic of grain boundary diffusion of
tracer with exchange.

boundaries to form new oxide at the oxide-metal interface. However, while diffusing down the grain boundaries the tracer comes into contact with the grains which have O-16 in them. This causes a tracer exchange between the grain boundaries and grains. It should be noted that the grains close to the gas surface have more tracer in them due to greater exchange time than the grains at the old-oxide new-oxide interface.

To model this process of grain boundary diffusion of tracer with exchange, the Oishi-Ichimura geometrical configuration has been chosen as shown in Figure 5. The polycrystalline oxide is assumed to consist of equal sized spherical grains and to possess a grain boundary diffusion coefficient that is much greater than the lattice diffusion coefficient. Diffusion of the tracer proceeds from the gas surface preferentially along the grain boundaries and from the grain boundaries radially inward towards the center of the grains. The grain boundaries of thickness are assumed to be perpendicular to the oxide surface . The grains of radius r are assumed to be attached to the grain boundaries at any arbitrary

O-18 TRACER

OLD OXIDE

(FORMED DURING
O-16 OXIDATION)

$J_{TOT} = J_y^{18}$

J_x^{18}
J_x^{16} — OXIDE GRAIN

δ

GRAIN BOUNDARY

$J_{TOT} = J_y^{18} + J_y^{16}$
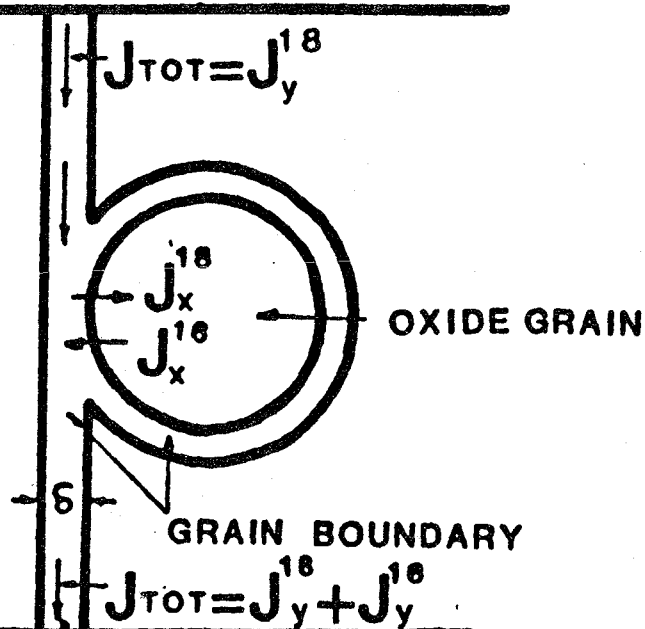
OXYGEN USED TO
FORM NEW OXIDE

NEW OXIDE

METAL

FIGURE 5 - Geometrical configuration of oxide grain and grain boundary.

depth in the oxide and are assumed to be completely surrounded by the grain boundaries. Basically, the grains act as sinks for the tracer and are attached to the grain boundary diffusion path. The complicated two dimensional combined lattice and the boundary diffusion problem is transformed into a simple one dimensional diffusion problem in the grain boundary with the grains acting as distributed sinks. The strength of the sinks is given by the well known case of diffusion into a sphere.

It should be noted that when the oxygen flux J^{TOT} enters the grain boundary at the gas surface, it is all O-18. However, as it comes in contact with a grain, there is a flux of tracer, J^{18}_x, into the grain due to exchange. However as the number of oxygen sites in the grains are fixed, there is an equal and opposite flux J^{16}_x of O-16 atoms out of the grain and into the grain boundary. Thus as the tracer diffuses down the grain boundary, it becomes more and more diluted in O-16 due to exchange. The grains act as a sink drawing O-18 atoms from the grain boundary and as a source supplying O-16 to the grain boundary. The grain
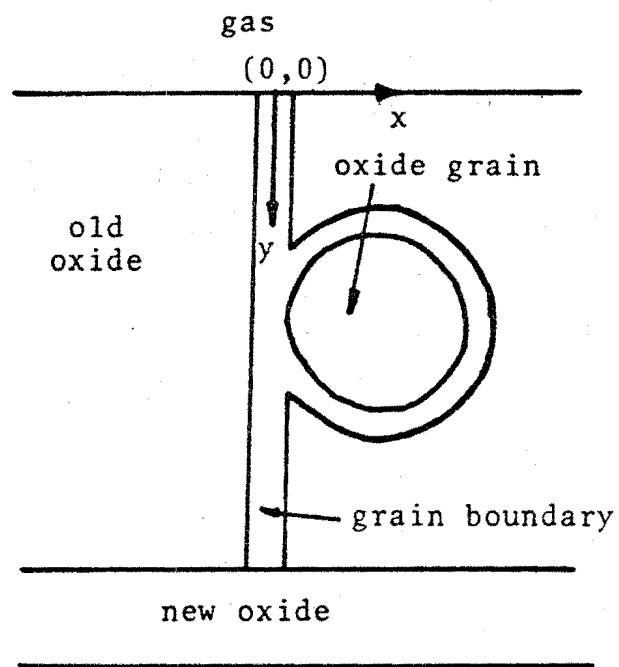
FIGURE 6 - Coordinate system for the model.

boundary oxygen flux at the old oxide-new oxide
interface which is used to form new oxide is
actually a mixture of tracer and natural oxygen.
This suggests that the isotopic content of the new
oxide grains preserves the information on the
amount of exchange occuring during the transport of
the tracer through the old oxide.

Figure 6 shows the coordinate system used in
the mathematical treatment of the diffusion
process. The list of symbols used are as follows.

J_y^{18} : Flux of tracer down the grain boundary (kg/m^2 sec)

J_x^{18} : Flux of tracer out of the grain boundary (kg/m^2 sec)

D_b : Grain boundary diffusion coefficient (m^2/sec)

D : Lattice diffusion coefficient (m^2/sec)

R : Gas constant (Joules/K mole)

T : Temperature (K)

μ^o : Oxidation chemical potential(Joules/K mole)

Y : Oxide thickness(m)

K_P : Parabolic rate constant for oxide growth(m^2/sec)

t : O-18 oxidation time (sec)

τ : O-16 oxidation time (sec)

ϕ_y : Tracer concetration in the grain boundary at depth y (kg/m^3)

C : Tracer concentration in the grain(kg/m^3)

C_i : Initial tracer concentration in the grain (kg/m^3)

$\bar{C}$: Average tracer concentration at depth y(kg/m^3)

δ : Grain boundary width (m)

r : Grain size (m)

$\bar{C}_s$: Average tracer concentration in oxide grain(kg/m^3)

3.5 Mathematical Modelling Of Diffusion

The flux of tracer down the grain boundary (J^{18}_y) is due to two gradients, the oxidation chemical potential gradient($\nabla \mu^o = \frac{\Delta \mu^o}{Y}$) which drives oxidation and its own concentration gradient($\frac{\partial \phi_y}{\partial y}$) due to isotopic mixing.

$$J^{18}_y = \frac{D_b \phi_y}{RT} \frac{\Delta \mu^o}{Y} - D_b \frac{\partial \phi_y}{\partial y} \qquad ...(3.1)$$

The diffusion coefficient D_b is different from the self diffusion coefficient of oxygen as jumps in the direction of the gradient are favoured. There is also a difference in correlation coefficients. However this difference in diffusion coefficient is small [43].

The flux of tracer out of the grain boundary and into the grain (J^{18}_x) is proportional to the concentration gradient of the tracer in the grain surface and the lattice diffuson coefficient D.

$$J^{18}_x = -D \left(\frac{\partial C}{\partial x} \right)_{x=\frac{\delta}{2}} \qquad ...(3.2)$$

The grain boundary is assumed to be thin enough to neglect the variation of ϕ_y in the x direction. Fick's second law gives the time dependence of the grain boundary tracer content.

$$\frac{\partial \phi_y}{\partial t} = -\frac{\partial J^{18}_y}{\partial y} - \beta \qquad ...(3.3)$$

41

where β is a sink term representing the rate of tracer loss into the grain. β is given by [5]:

$$\beta = \frac{2}{\delta} J_x^{18} \qquad \qquad ...(3.4)$$

Substitution of the Equation 3.2 in Equation 3.4 gives:

$$\beta = -\frac{2D}{\delta} \left(-\frac{\partial C}{\partial x}\right)_{x=\frac{\delta}{2}} \qquad ...(3.5)$$

Thus the time dependence of the tracer content in the grain boundary is given by substituting Equation 3.1 and Equation 3.5 in Equation 3.3.

$$\frac{\partial \phi_y}{\partial t} = -\frac{D_b \Delta \mu^o}{RT\ Y}\frac{\partial \phi_y}{\partial y} + D_b\frac{\partial^2 \phi_y}{\partial y^2} + \frac{2D}{\delta}\left(\frac{\partial C}{\partial x}\right)_{x=\frac{\delta}{2}} \ ...(3.6)$$

The last term of the Equation 3.6 can be evaluated if the concentration gradient of the tracer at the grain surface is known. The increasing rate of the grain boundary concentration is much larger than the increasing rate of the tracer concentration within the grain for a given time, since the grain boundary diffusion coefficient is much larger than the lattice diffusion coefficient. Thus the concentration variation within the grain can be considered for a constant ϕ_y with a relatively small error. Thus the problem of tracer exchange reduces to the standard problem of diffusion into a sphere having a constant surface concentration ϕ_y .

The standard solution to this equation is given in Equation 3.7.

$$\frac{C-C_1}{\phi_y-C_1} = 1 + \frac{2r}{\pi(r-x)} \sum_{n=1}^{\infty} \frac{(-1)^n}{n} \sin\frac{n\pi(r-x)}{r} \exp(\frac{-Dn^2\pi^2 t}{r^2}) \quad \ldots(3.7)$$

Differentiation of Equation 3.7 by x gives Equation 3.8, an expression for the tracer concentration gradient at the grain surface (if $\delta \ll r$).

$$(\frac{\partial C}{\partial x})_{x=\frac{\delta}{2}} = -(\phi_y-C_1)\frac{2}{r} \sum_{n=1}^{\infty} \exp(\frac{-Dn^2\pi^2 t}{r^2}) \quad \ldots(3.8)$$

Substitition of Equation 3.8 in Equation 3.6 gives Equation 3.9.

$$\frac{\partial\phi_y}{\partial t} = -\frac{D_b\Delta\mu^o}{RT~Y}\frac{\partial\phi_y}{\partial y} + D_b\frac{\partial^2\phi_y}{\partial y^2} - \frac{4D}{r}(\phi_y-C_1) \sum_{n=1}^{\infty} \exp(\frac{-Dn^2\pi^2 t}{r^2}) \quad \ldots(3.9)$$

This is a differential equation involving only the grain boundary concentration and its variation in the y direction and time. The scale thickness is time dependent. So if a parabolic growth rate is assumed with K_p as the parabolic rate constant,

$$Y = (K_p(t+\tau))^{1/2} \quad \ldots(3.10)$$

where t and τ are the O-18 and O-16 oxidation times respectively. Equation 3.9 can thus be written as:

$$\frac{\partial\phi_y}{\partial t} = D_b\frac{\partial^2\phi_y}{\partial y^2} - \frac{D_b\Delta\mu^o}{RT(K_p(t+\tau))^{1/2}}\frac{\partial\phi_y}{\partial y} - \frac{4D}{r\delta} \sum_{n=1}^{\infty} \exp(\frac{-Dn^2\pi^2 t}{r^2})\phi_y$$

$$+ \frac{4DC_1}{r\delta} \sum_{n=1}^{\infty} \exp(\frac{-Dn^2\pi^2 t}{r^2}) \quad \ldots(3.11)$$

This differential equation can be easily solved

numerically to give the grain boundary tracer concentration $\phi_y(y,t)$. Note that ϕ_y depends upon three transport parameters D, δ and D, the oxide microstructure through the grain size r and the oxide growth kinetics through the parabolic constant K_p. When Equation 3.11 is divided by the total oxygen concentration in kg/m^3, which is the same throughout the oxide scale, the tracer concentration can be converted from kg/m^3 to fractional oxygen concentration. Thus C, C_i and ϕ_y all become unitless and are actally:

<u>kg of tracer per cubic meter</u>
kg of oxygen per cubic meter

As the SIMS determines the tracer concentration profile by the sectioning technique, the average concentration of the tracer at any depth y should be determined. The average tracer concentration in the oxide grain at depth y at a time t is given by [11]

$$\overline{C}_g = \frac{M_t}{M_\infty} (\phi_y - C_i) + C_i \qquad \ldots (3.12)$$

where M_t and M_∞ are the total amounts of tracer diffusing into the grain at times t and ∞, respectively. $\frac{M_t}{M_\infty}$ is not a function of the grain

44

boundary diffusion coefficient D_b but only of the lattice diffusion coefficient D and is given by the standard form [11]:

$$\frac{M_t}{M_\infty} = 1 - \frac{6}{\pi^2} \sum_{n=1}^{\infty} \frac{1}{n^2} \exp(\frac{-Dn^2\pi^2 t}{r^2}) \quad \ldots (3.13)$$

Thus $\overline{C}_s$ can be written as:

$$\overline{C}_g = (1 - \frac{6}{\pi^2} \sum_{n=1}^{\infty} \frac{1}{n^2} \exp(\frac{-Dn^2\pi^2 t}{r^2}))(\phi_y - C_i) + C_i \quad \ldots (3.14)$$

If the contribution of the tracer in the grain boundary is considered, the average tracer concentration at depth y and time t is given by:

$$\overline{C}(y,t) = \frac{\frac{4}{3}\pi r^3 \overline{C}_g + 4\pi r^2 \frac{\delta}{2} \phi_y}{\frac{4}{3}\pi r^3 + 4\pi r^2 \frac{\delta}{2}} \quad \ldots (3.15)$$

Due to the rastering technique $\overline{C}(y,t)$ is the quantity measured by SIMS:

3.6 Boundary Conditions

Equation 3.11 is solved by a numerical solution using the finite difference method. (y,t) is determined by using the first central difference form of the derivatives [45]. If X is the thickness of the old oxide and Y(t) is the total thickness of the oxide at any time t, the initial conditions are:

$$\phi_y = C_i \ , \ y \leqslant X \ , \ t = 0$$
$$C = C_i \ , \ 0 < x < r \ , \ y \leqslant X \ , \ t = 0 \qquad \ldots (3.16)$$

45

It is assumed that the natural isotopic concentration of the tracer is negligible i.e.,

$$C_i = 0 \qquad \qquad ...(3.17)$$

The boundary condition at the oxide-gas interface is:

$$\phi_y = C_s \ , \quad t>0 \ , \quad y=0 \qquad \qquad ...(3.18)$$

where C_s is the tracer concentraton in the gas during the O-18 oxidation. C_s is assumed to be constant during the diffusion.

The oxide-metal interface is a moving boundary. As new oxide is being formed at the oxide-metal interface due to the flux of tracer through the grain boundaries, the tracer concentration in the new oxide grains being formed is the same as the grain boundary tracer concentration at the metal-oxide interface. Figure 7 shows the new oxide growth ΔY during the time Δt. The boundary conditions at this interface are:

$$C(0<x<r, \ Y<y<Y+\Delta Y, \ t=t+\Delta t) = \phi_y(y=Y, \ t=t+\Delta t)$$

$$\phi_y(Y<y<Y+\Delta Y, \ t=t+\Delta t) = \phi_y(y=Y, \ t=t+\Delta t) \qquad ...(3.19)$$

where limit : $\quad \Delta Y, \Delta t \rightarrow 0$

In the following section some of the quantities necessary for the numerical solution of Equation 3.11 will be determined.
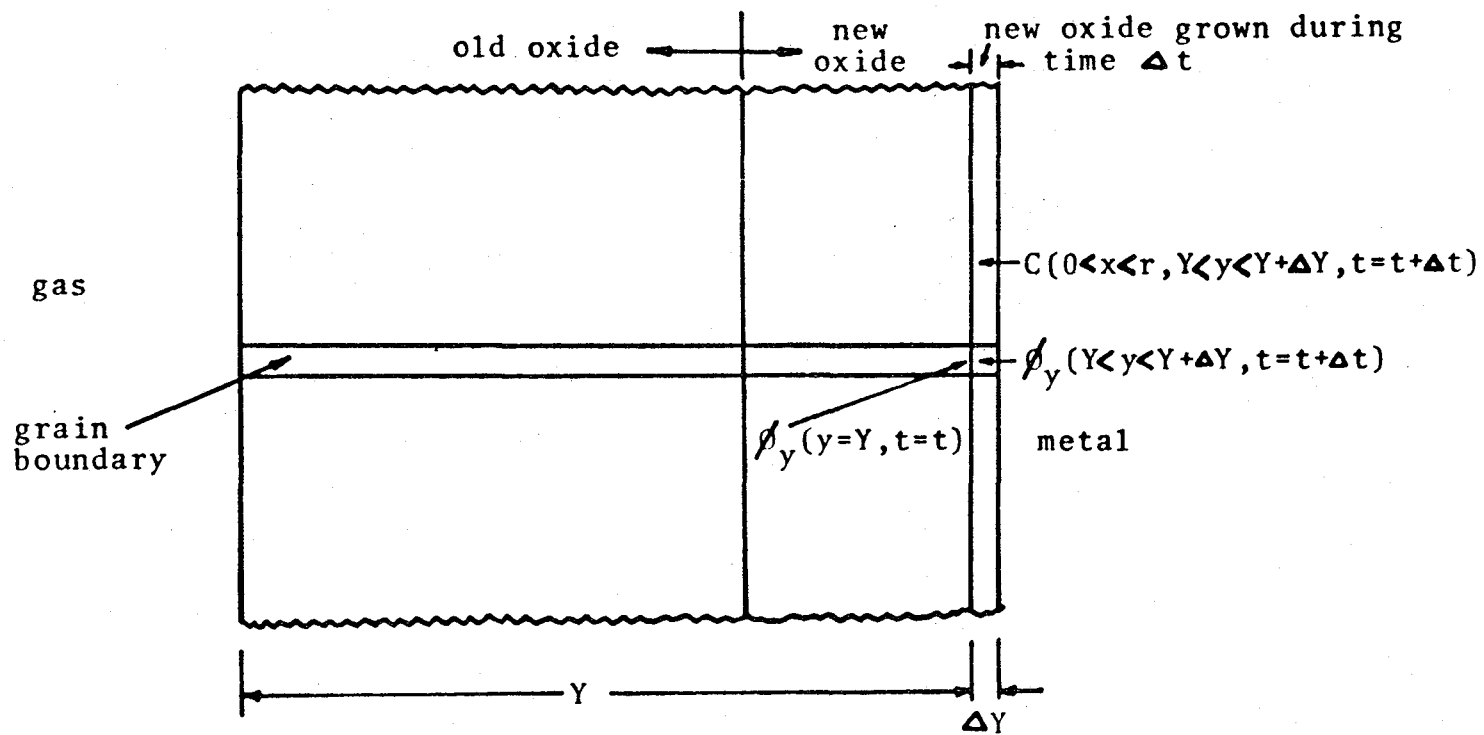
FIGURE 7 - Boundary conditions at the oxide-metal moving boundary.

3.7 Determination of oxidation chemical potential gradient

Let the gas oxide interface be denoted as 1 and the oxide metal interface be denoted as 2 as shown in Figure 8. Let $\mu_{O_2}^1$ and $\mu_{O_2}^2$ be the oxygen chemical potential in the oxide at 1 and 2 respectively. At 1 the chemical potential of oxygen in the gas must be the same as the chemical potential in the oxide [46] i.e.,

$$\mu_{O_2}^1 = \mu_{O_2}^{gas}$$

As the sample is exposed to a closed atmosphere of pure oxygen during the tracer oxidation,
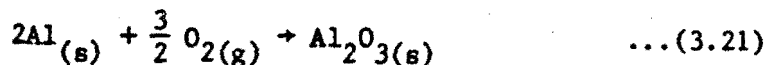
$$p_{O_2}^{gas} = 1$$

This gives

$$\mu_{O_2}^1 = \mu_{O_2}^{gas} = RT \ln p_{O_2}^{gas} = 0 \qquad ...(3.20)$$

i.e., we choose the standard state as 1 atmosphere oxygen gas. At 2 the oxygen chemical potential must be the same at the oxide and the metal i.e.,

$$\mu_{O_2}^2 = \mu_{O_2}^{metal}$$

At 2 the reaction:

$$2Al_{(s)} + \frac{3}{2} O_{2(g)} \rightarrow Al_2O_{3(s)} \qquad ...(3.21)$$
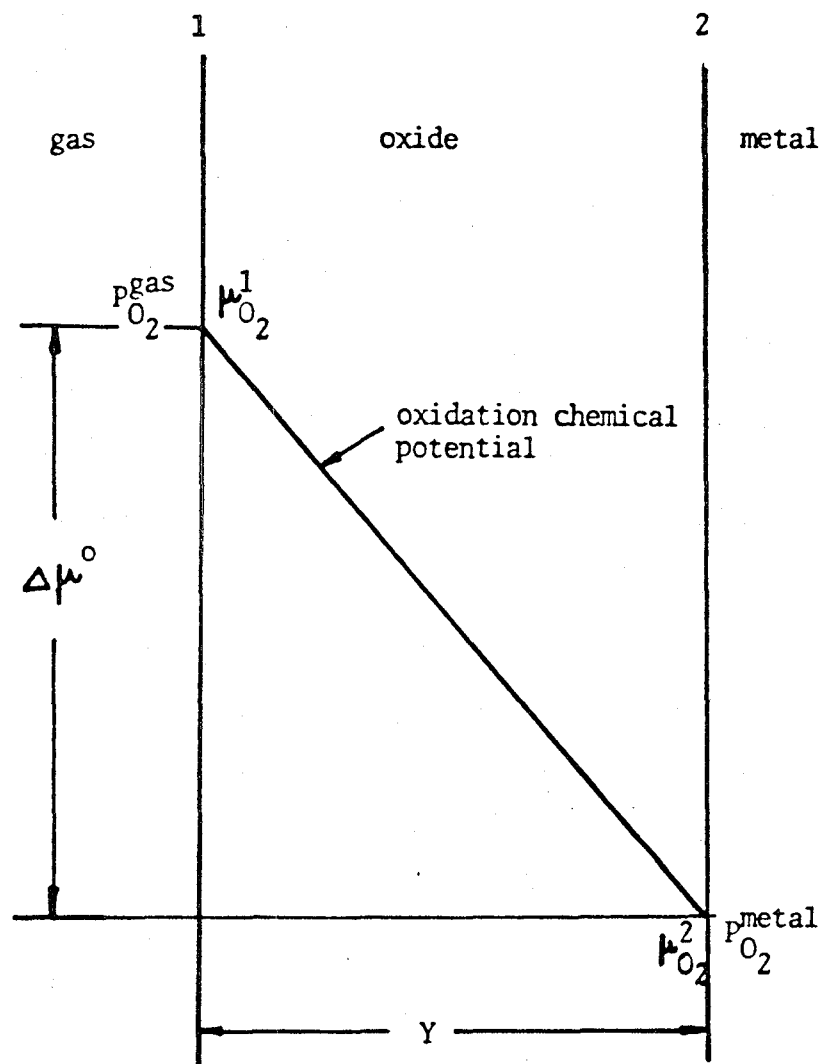
48

FIGURE 8 - Oxidation chemical potential gradient across the oxide scale.

takes place which has a free energy change of   .
An equilibrium constant K for this reaction can be
defined as:

$$\Delta G^o = -RT \ln K = -RT \ln \frac{a_{Al_2O_3}}{(a_{Al})^2 (a_{O_2}^{metal})^{3/2}} \quad ...(3.22)$$

$a_{Al_2O_3}$ can be assumed to be unity. Thus Equation
3.22 becomes:

$$a_{O_2}^{metal} = \exp(- \frac{2}{3} \frac{|\Delta G^o|}{RT})(a_{Al})^{-4/3} \quad ...(3.23)$$

Since $\mu_{O_2}^{metal} = RT \ln a_{O_2}^{metal}$, Equation   3.23
gives:

$$\mu_{O_2}^{metal} = - \frac{2}{3} |\Delta G^o| - \frac{4}{3} RT \ln (a_{Al}) \quad ...(3.24)$$

In the absence of any thermodynamic activity data,
the metal can be assumed to be a single phase ideal
solution. Then a   is the atomic percent of
              Al
aluminum in the alloy ; [Al]. Thus the Equation
3.24 becomes:

$$\mu_{O_2}^2 = \mu_{O_2}^{metal} = - \frac{2}{3} |\Delta G^o| - \frac{4}{3} RT \ln [Al] \quad ...(3.25)$$

Thus the oxidation chemical potential difference
across the oxide scale is given by:

$$\Delta\mu^o = \mu_{O_2}^1 - \mu_{O_2}^2 = \frac{2}{3} |\Delta G^o| + \frac{4}{3} RT \ln [Al] \quad ...(3.26)$$

Substitution of values of   and [Al] in Equation
3.26 gives: $\Delta\mu^o = 787915$ J/mole at 1100^oC.

3.8 Relationship between D_b and K_p

If the mechanism of oxide growth is primarily inward oxygen diffusion through the grain boundaries, the grain boundary diffusivity and the growth rate kinetics can be related by considering a simple model.

The sample is exposed to natural oxygen and an oxide scale is grown. The oxide is assumed to have cubic grains of dimension r surrounded by the grain boundaries of thickness δ as shown in Figure 9. The cross section of the sample itself is assumed to be a square with each side being n grains long. Let the thickness of the oxide at any time t be Y and let the scale grow by an amount ΔY in time dt. Then the flux of oxygen J^o $(kg/m^2 sec)$ down the grain boundaries is due to the oxygen potential gradient.

The amount of oxygen transferred in time through the grain boundaries, W_T^o (kg) is given by:

$W_T^o = J^o$. area of grain boundaries . time

the shaded area in Figure 9 is the grain boundary area through which the oxygen is transported($\delta \ll r$).

$$W_T^o = \frac{D_b C}{RT} \frac{\Delta \mu^o}{Y} . 2n^2 r\delta . \Delta t \qquad \qquad ...(3.27)$$
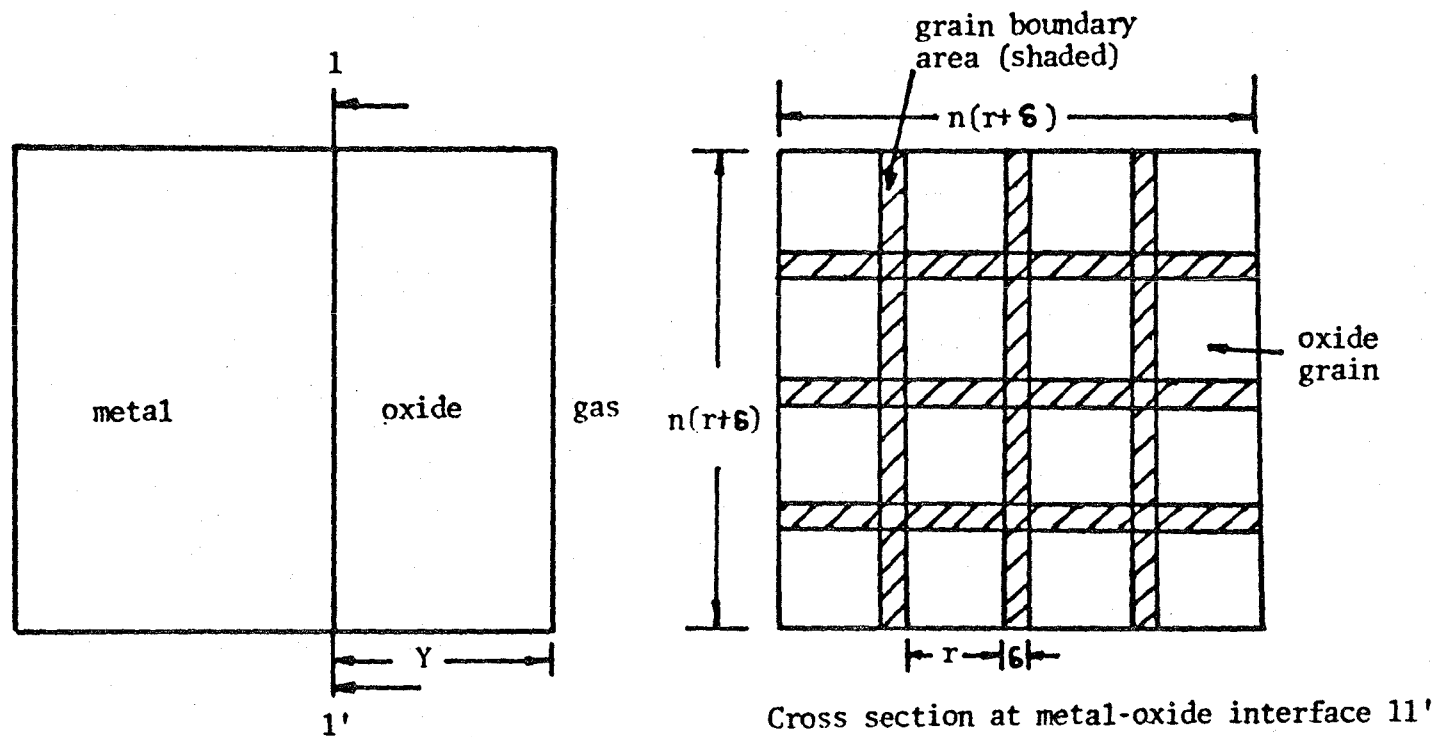
FIGURE 9 - Schematic of model geometry used to relate scale growth kinetics to grain boundary diffusion.

This amount of oxygen transported must be the same as the amount of oxygen incorporated in the net growth of oxide, W_N^o (kg).

W_N^o = volume of new growth in time Δt . concentration of O in scale

$$W_N^o = (nr)^2. \; \Delta Y \; . \; C \qquad\qquad ...(3.28)$$

where C is the oxygen concentration (kg/m^3) in the scale. As $W_T^o = W_N^o$, Equation 3.27 and Equation 3.28 gives:

$$\frac{D_b C}{RT} \frac{\Delta \mu^o}{Y} \; 2n^2 \; r \; \delta \; \Delta t = n^2 r^2 \; \Delta Y \; C$$

$$\Rightarrow \frac{2\delta D_b \Delta \mu^o}{RT \; r \; Y} = \frac{\Delta Y}{\Delta t} \qquad\qquad ...(3.29)$$

$\frac{\Delta Y}{\Delta t}$ is the growth rate of the oxide. If a parabolic growth rate is assumed with growth rate constant K_p

$$Y = (K_p t)^{1/2}$$

$$\Rightarrow \frac{dY}{dt} = \frac{1}{2} K_p^{1/2} \; t^{-1/2} \qquad\qquad ...(3.30)$$

Combining Equations 3.29 and 3.20 gives:

$$\delta D_b = (\frac{rK_p}{4}) \frac{RT}{\Delta \mu^o} \qquad\qquad ...(3.31)$$

Substitution of appropriate values in Equation 3.31: r=0.3 microns, T=1100 ^{o}C , K_p =1.2x10^{-16} m^2/sec , δ =10 A , $\Delta \mu^o$=78915 J/mole gives:

$$D_b = 1.3 \times 10^{-16} \, m^2/sec \qquad \qquad \ldots(3.32)$$

This gives a good estimate of the value of D_b to be used in the numerical solution of the Equation 3.11.

3.9 Tracer concentration profile in the new oxide

The tracer concentration profile in the new oxide is obtained by the principle of mass balance. It is assumed that the amount of exchange of O-16 in the oxide grains at the gas surface with the O-18 in the tracer due to volume diffusion at the gas-oxide interface is negligible. Then for an inward growing scale once the sample is exposed to pure tracer, the amount of O-16 in the entire oxide must remain constant. This means that the amount of O-18 retained in the old oxide must be the same as the amount of O-16 in the new oxide. Let X be the thickness of the oxide after an O-16 oxidation for time τ and let Y be the oxide thickness after a further tracer oxidation for a time t. Let an additional tracer oxidation for a time dt cause a new oxide growth of dY as shown in Figure 10. The tracer concentration profile till depth Y at time t+dt is also shown.
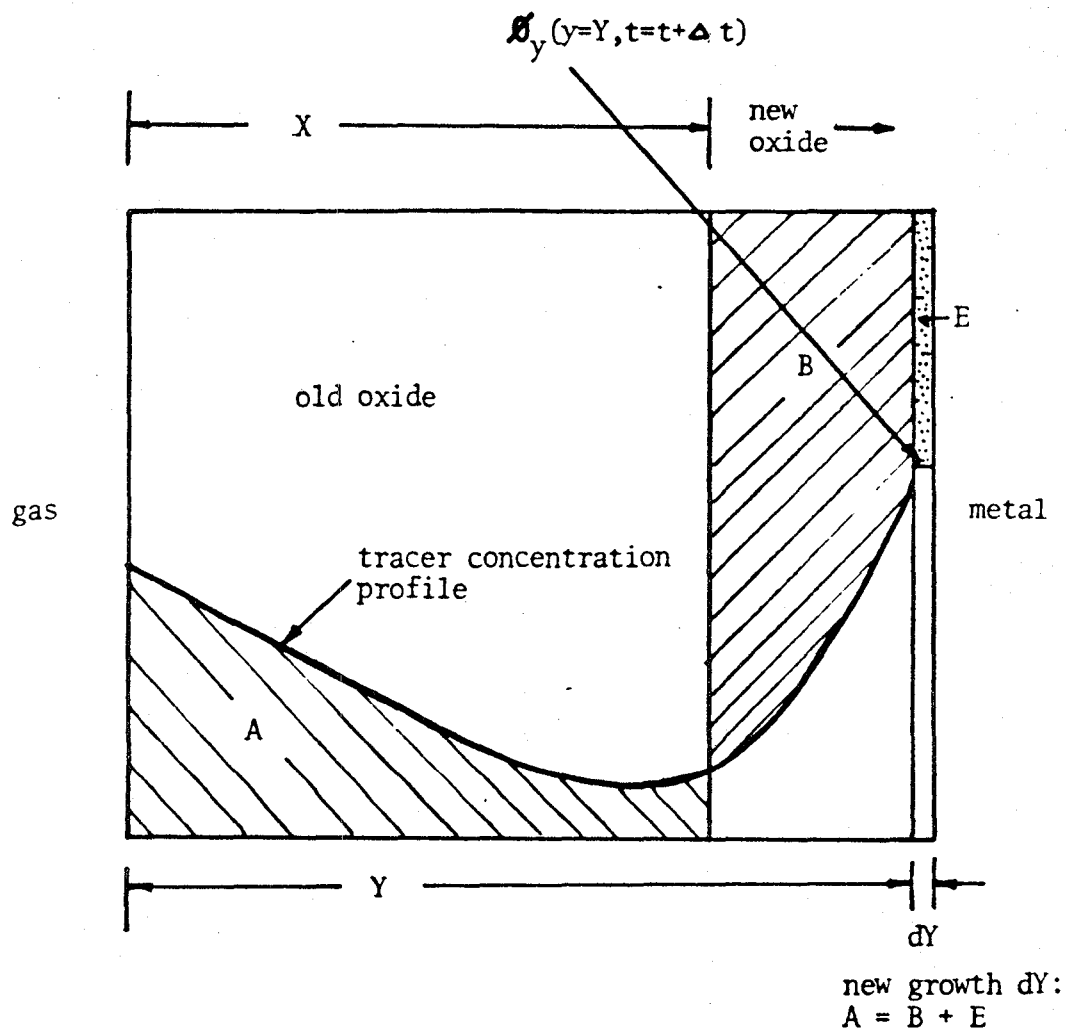
FIGURE 10 - Determination of oxide growth kinetics by mass balance.

Area A denotes the amount of tracer in the old
oxide and area B denotes the amount of O-16 in the
new oxide grown till time t. Let A-B=E. Then by
mass balance, the amount of O-16 contained in the
new growth dY must be E. As mentioned in Section
3.6, the tracer concentration in the new growth is:

$$\phi_y = (y{=}Y, \ t{=}t{+}\Delta t)$$

which gives the O-16 concentration in the new
growth as: $\quad (1 - \phi_y(y{=}Y, \ t{=}t{+}\Delta t)$

Thus the growth dY during time dt can be calculated
as:

$$dY = \frac{(A-B)}{(1-\phi_y(y=Y,t=t+\Delta t))} \qquad \ldots(3.33)$$

3.10 Flow chart of computer solution

Equation 3.11 is solved on the computer using
the finite difference technique. The old oxide is
divided into 19 equal parts with the oxide-gas
interface being called 1 and the metal-oxide
interface being called 20, as shown in Figure 11.
Each part is considered to be 1 unit. The growth
rate of the oxide is determined by mass balance as
discussed in Section 3.9. The value of D_b is
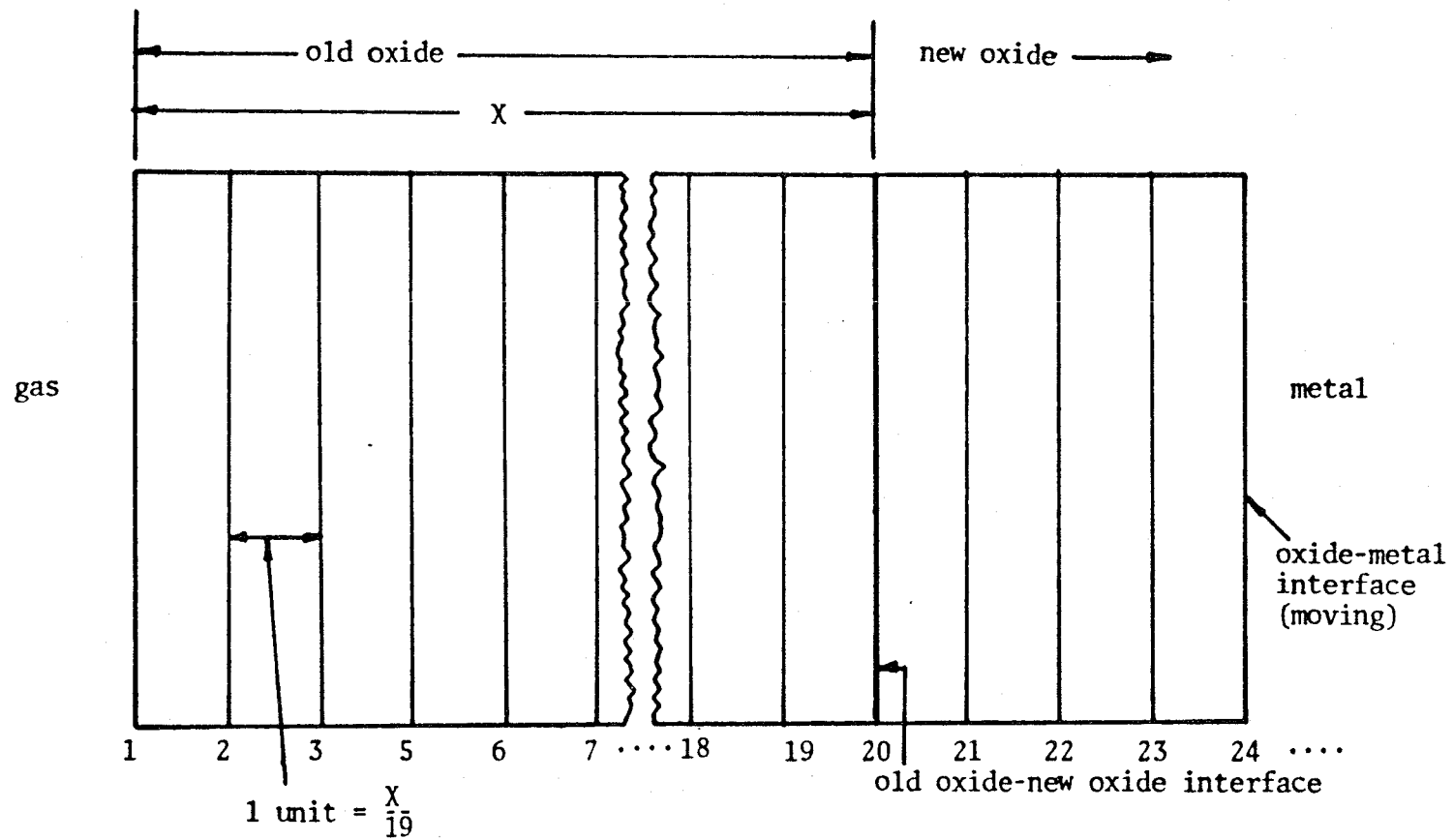chosen such that the growth rate is compatable

FIGURE 11 - Division of oxide scale for finite difference solution.

57

with the parabolic growth rate kinetics. The flow chart for the computer program is shown in Figure 12. The computer program is listed in appendix A.

3.11 Computer plots of tracer profiles

Figures 13-15 show the theoretical tracer concentration profiles in the old oxide for various values of lattice diffusivity, grain boundary diffusivity and grain size. A higher value of lattice diffusivity and causes a fast exchange rate to be set up. The grains in the old oxide are filled up quickly. A higher value of the grain boundary diffusivity causes more tracer to be retained in the grains of the old oxide as the tracer diffuses quickly down the grain boundaries increasing the exchange time for the grains. A smaller grain size increases the surface area for exchange and causes more tracer to be retained in the old oxide. The variation of the tracer profiles when each parameter is varied is different. Thus theoretically given an experimental tracer profile, it should be possible to come up with unique values of the three parameters to fit the curve. It should be noted that the values of D_b and r are
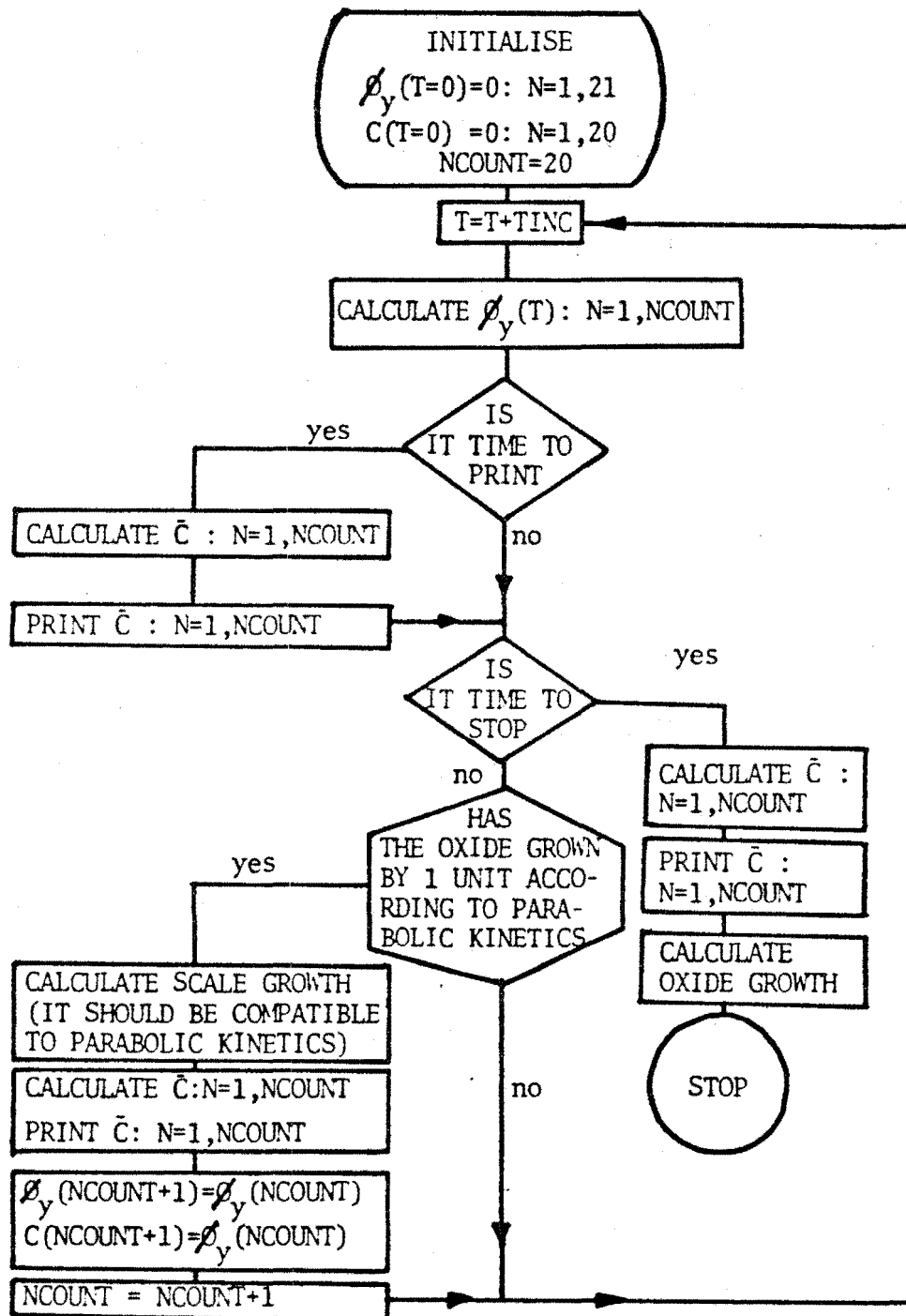
FIGURE 12 - Flow chart for the computer program.

O-16 oxidation time- 18 hours
O-18 oxidation time- 14 hours
at $1100^{\circ}C$
$D_b = 1.3 \times 10^{-16} m^2/sec$
grain size=0.3 microns
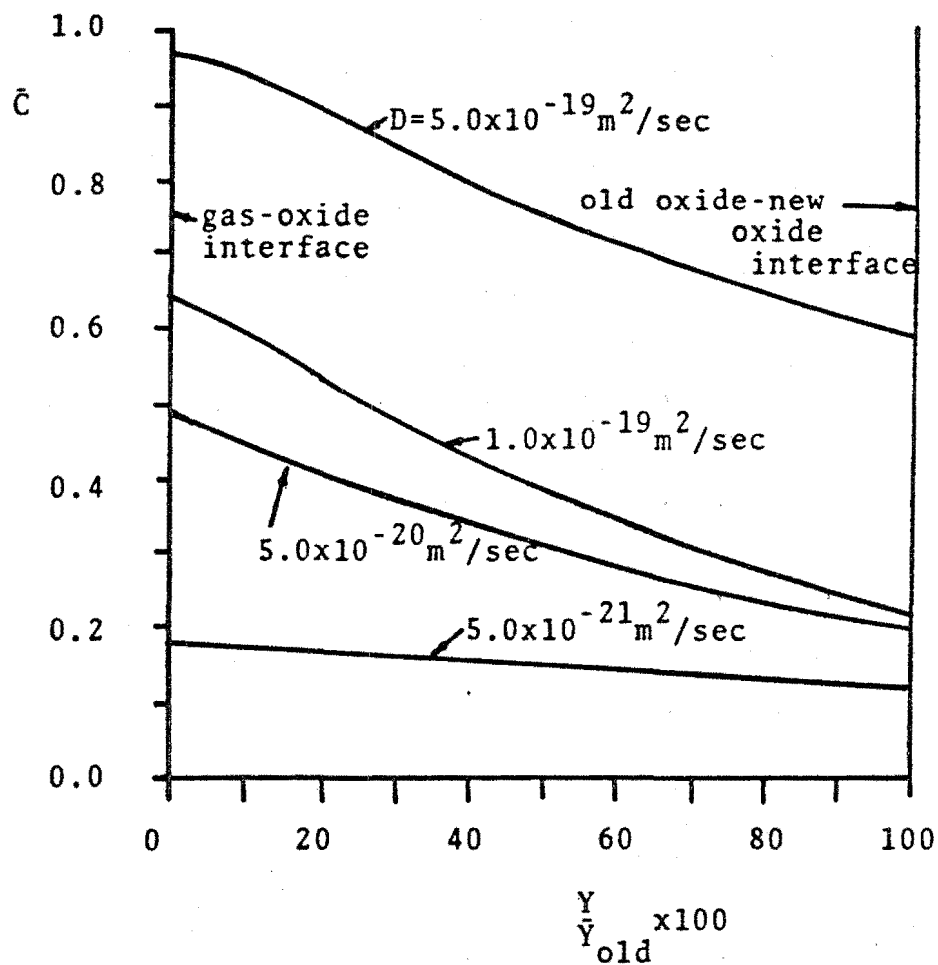
FIGURE 13 - Effect of lattice diffusion coefficient
on the tracer profile in the old scale.

O-16 oxidation time-18 hours
O-18 oxidation time-14 hours
at $1100^{\circ}C$
$D=5.0 \times 10^{-20} m^2/sec$
grain size=0.2microns

$\bar{C}$

oxide-gas interface

old oxide-new oxide interface

$D_b = 5.0 \times 10^{-16} m^2/sec$

$1.3 \times 10^{-16} m^2/sec$

$5.0 \times 10^{-17} m^2/sec$

$\dfrac{Y}{Y_{old}} \times 100$
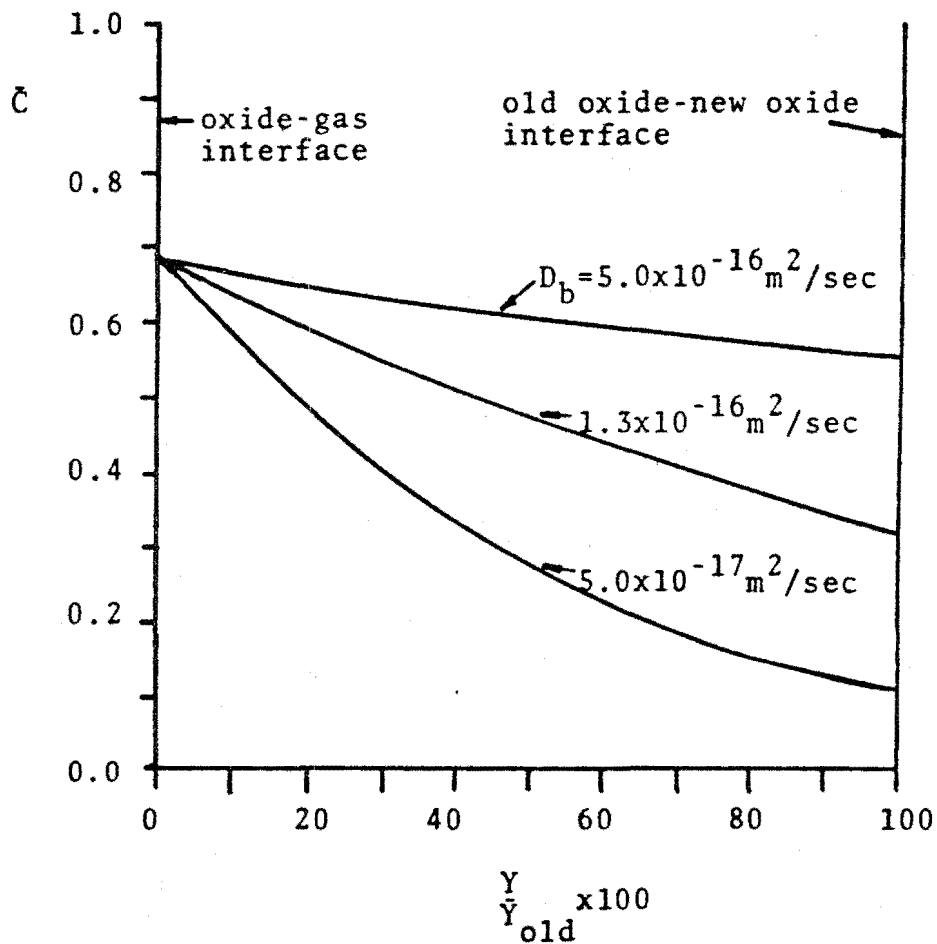
FIGURE 14 - Effect of grain boundary diffusion coeffi-
cient on the tracer profile in the old
scale.

61

O-16 oxidation time-18 hours
O-18 oxidation time-14 hours
at 1100°C
$D_b = 1.3 \times 10^{-16} m^2/sec$
$D^b = 5.0 \times 10^{-20} m^2/sec$

$\bar{C}$

oxide-gas
interface

old oxide-new
oxide inter-
face

grain size=0.2microns

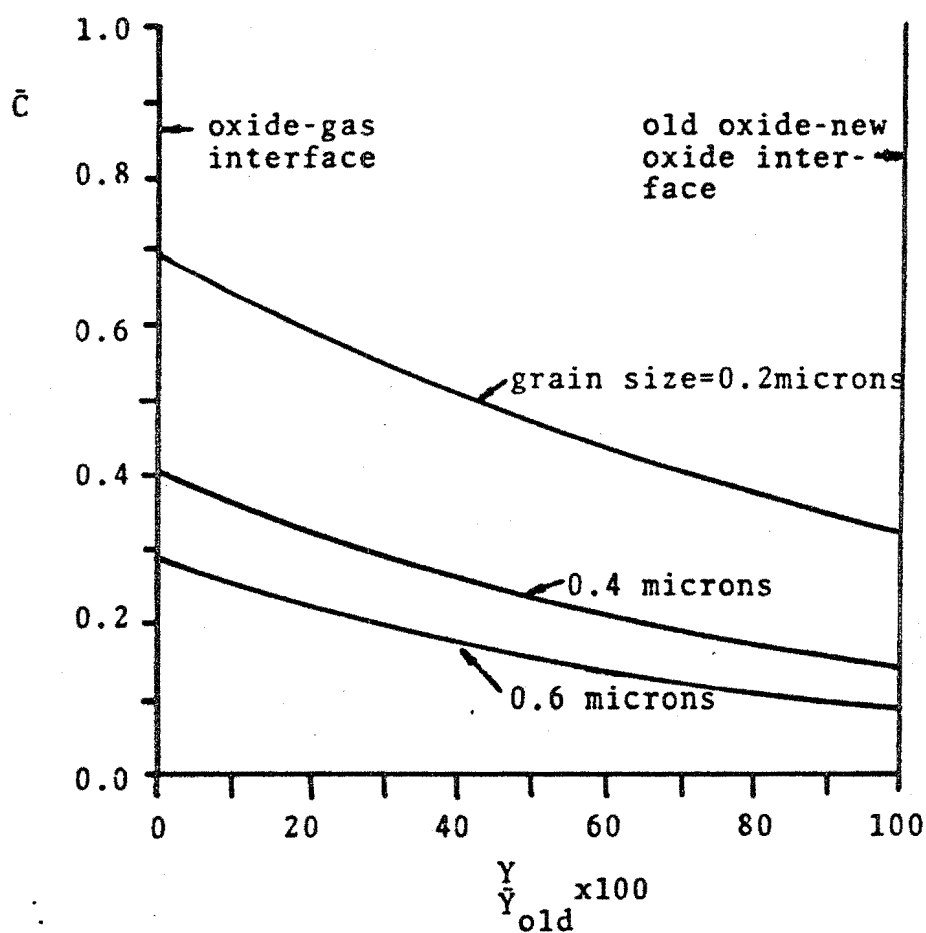0.4 microns

0.6 microns

$\frac{Y}{Y_{old}} \times 100$

FIGURE 15 - Effect of grain size on the tracer profile
in the old scale.

not independent, but are related to the K value by
Equation 3.31. Thus if one of the above parameters
is fixed, there is a unique value of the other
parameter to satisfy the parabolic growth rate
kinetics. Figures 13-15 are plotted to show how
sensitive the profiles are to the three parameters.

Figure 16 shows the computer simulation of how
the tracer concentration profile develops accross
the entire oxide scale when the scale grown by a
18 hour O-16 oxidation followed by a 14 hour O-18
oxidation. The values of the three parameters
chosen are:

$$D_b = 1.41 \times 10^{-16} \ m^2/sec, \quad D = 10^{-20} \ m^2/sec$$

$r = 0.3$ microns

The value of the grain boundary width chosen is
$10\overset{o}{A}$.

Here we can see the versatility of the model.
The oxide microstructure can be incorporated in the
program by feeding in the real grain size variation
across the scale. In case the lattice diffusion
coefficient varies across the side, that too can be
incorporated in the program. The actual value of

63

O-16 oxidation time = 18 hours
1 unit = X/19

a) O-18 oxidation time = 4 hours

b) O-18 oxidation time = 8 hours, 25 minutes
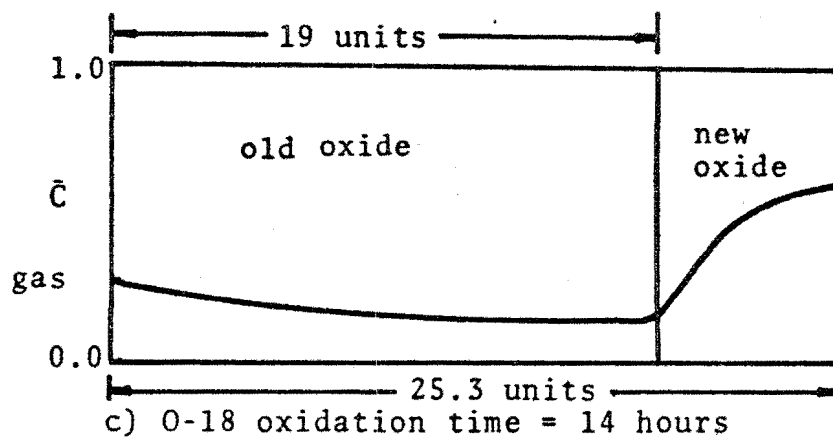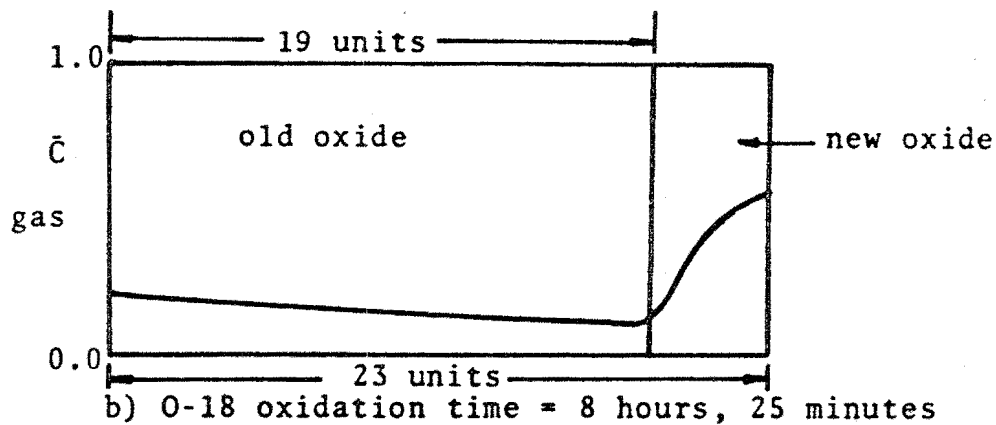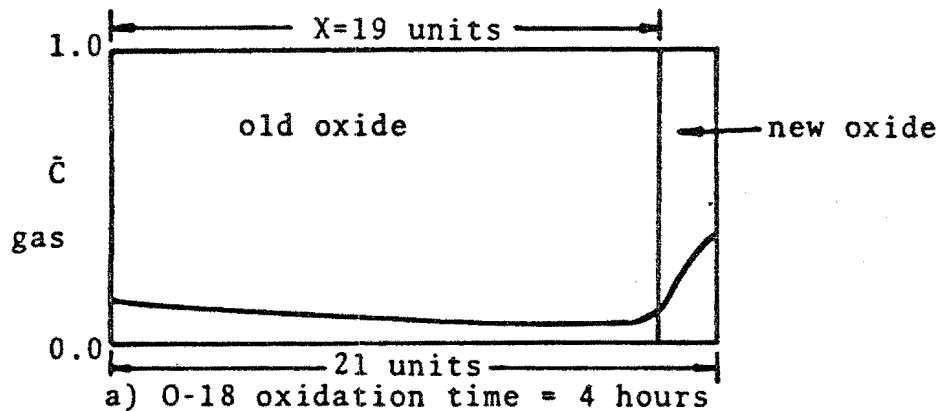

c) O-18 oxidation time = 14 hours

FIGURE 16 - Development of tracer concentration profile.

the oxide growth kinetics can be experimentally found and the real value of Y(t) can be used in the program. The value of D_b can be so adjusted that the growth rate predicted by mass balance is the same as the experimental growth rate. So long as the oxide is inward growing, the tracer profile for any growth kinetics and microstructure can be modelled.

It should be noted that the model is based on a planar oxide growth mechanism and any quantitative information derived from the experimental profiles assumes good resolution and high quality of the data itself. In case the oxide metal interface is irregular, it is difficult to identify the interface for the purpose of mass balance. The same problem arises if the sputtering itself is non uniform and information at the metal-oxide interface is being gathered simultaneously from both metal and oxide grains. Non uniform sputtering can severly limit the resolution of the data such that no quantitative information can be obtained from the shape of the profile.

CHAPTER 4

EXPERIMENTAL PROCEDURE

4.1 Sample Preparation

The FeCrAl-Zr alloy used in the experiment
was obtained through NASA Lewis Research Center.[*]
The alloy used was Fe-21.9Cr-5.8Al-0.22Zr and was
obtained as cold rolled strips about 1.5mm thick.
Samples of size 6mmx6mmx1.5mm were cut out by a
Buehler diamond saw. The specimens were then
mounted and polished on 240,320 and 600 grit
polishing paper followed by 15,3 and 1 micron
diamond paste polishing. Some of the samples were
prepared at NASA and were polished by 600 grit
polising paper followed by 3 micron and 1 micron
diamond paste polish. .

4.2 Exchange Apparatus

Figure 17 shows a schematic of the apparatus
used for the gas exchange process. The tracer is
kept in a zeolite storage tank.

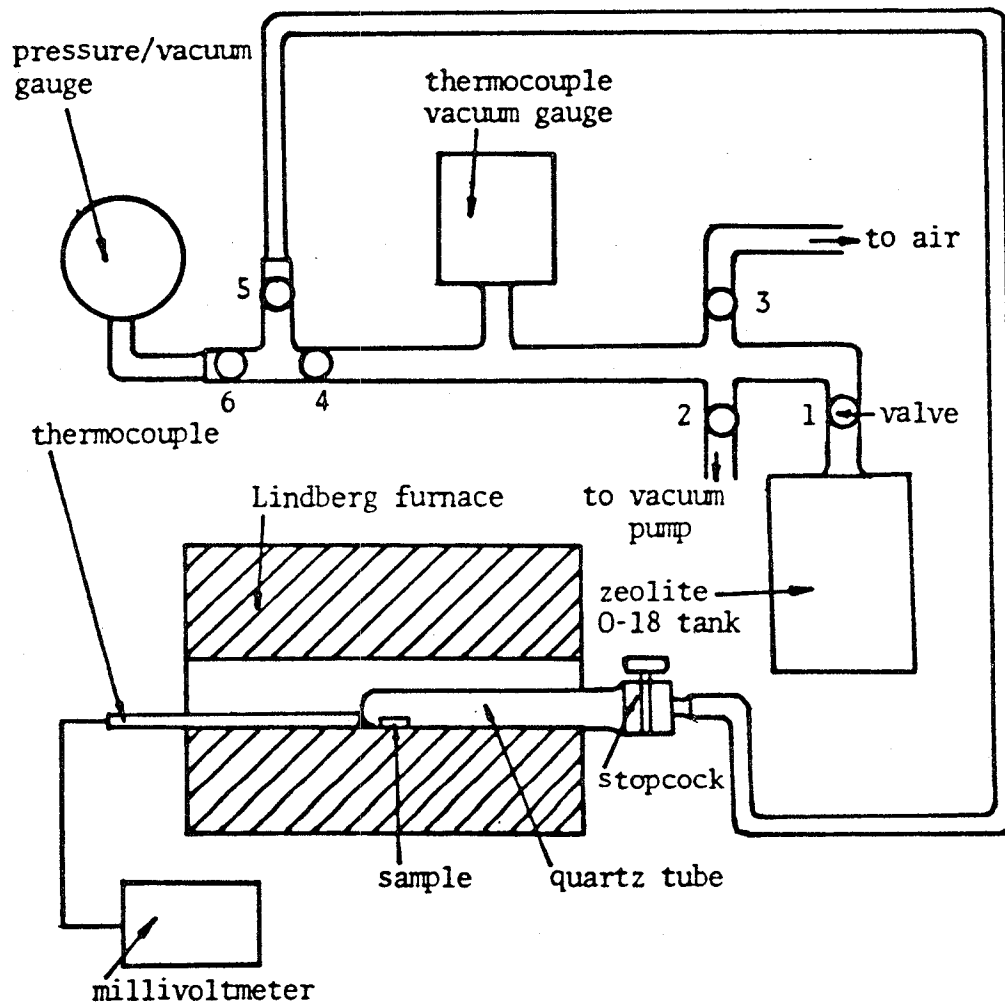
* Courtsey J.Smialek.

66

FIGURE 17 - Schematic of gas exchange apparatus.

The sample is placed in a quartz tube with the polished side up. Oxygen flow into the quartz tube can be controlled by valve 5 and the stopcock. The thermocouple vacuum gauge measures the pressure inside the system when it is evacuated. The pressure gauge measures the pressure in the system when the tracer is introduced. Normally the tracer pressure in the system is maintained slightly above the atmospheric pressure such that no air leaks into the system during the tracer anneal. The sample is annealed by placing the quartz tube in a single zone horizontal Lindberg furnace. The temperature of the furnace is monitored by a Pt-6%/Rh/Pt-30%Rh thermocouple.

4.3 Exchange Procedure

Some of the samples are annealed in vacuum after polishing to remove the polising damage. The samples are placed in the quartz tube and the system is pumped down to a pressure of 0.03torr. The samples are then annealed at $1100\ ^{\circ}C \pm 5\ ^{\circ}C$ for 30 minutes. This also helps the sample and the quartz tube to heat up and come into thermal

equilibrium with the furnace. For the O-16 anneal, valve 2 is closed to cut off the vacuum pump and valve 3 is opened to introduce air into the system. So the old scale is grown in air at 1 atmosphere pressure. The transfer of O-18 into the system for the tracer anneal is done without cooling down the system. At the end of O-16 anneal, valve 3 is closed and the system is evacuated with the vacuum pump by opening valve 2. Meanwhile the temperature of the zeolite tank is raised by using the heating coil. When the pressure of the system falls to 0.03 torr, valve 2 is closed and the tracer is introduced into the system through valve 1. The O-18 is kept at a slightly higher than atmospheric pressure to ensure no leakage of atmospheric air into the system which can cause dilution of the tracer. At the end of the tracer anneal, the system is evacuated again by cooling the zeolite tank with liquid nitrogen. On cooling it acts as a pump and sucks out all the tracer from the system.

4.4 SIMS

The GATAN SIMS at Pennsylvania State University* was used to obtain the data for the tracer concentration profile. The primary beam used was Ar$^+$ under a beam acceleration voltage of 7KV. The complete instrument settings are listed below:

Beam Acclerator	7 KV	1.53 mA
Ion Source Filament		17.2 A
Anode	123 V	3.65 mA
Beam Deflector	Initial - 43 V	Final - 204 V
Lens Control Condensor	6.16 KV	
Velocity filter	Electric Field-	0.81 V
	Magnetic field-	0.59 A
	Objective -	4.18 KV
Energy filter	Outer potential-	40 V
	Inner potential-	113 V
	Bias -	39 V

----

* Operated by Dr.C.Hauser under the guidance of Prof.C.Pantano.

70

The list of species simultaneously monitored and
their mass to charge ratio is given below:

Element	Mass/Charge ratio monitered
Al	13.9
^{16}O	16.4
^{18}O	18.4
Cr	52.9
Fe	56.9
Zr	91.7

Due to the insulating properties of alumina,
it was necessary to compensate for the positive
charge of the primary beam by spraying electrons
on the sample surface. These electrons can cause
desorpton of light elements from the near surface
region. This gives rise to a background intensity
of the monitored ions and is termed as Electron
Stimulated Desorption(ESD). The ESD level is
evaluted by shutting off the primary beam and
measuring the secondary ions due to the electron
beam only. This background level is subtracted
out from the actual reading.

A sample holder for SIMS can hold upto 6 samples and has in addition 2 standards. The first standard is Ta_2O_5 on Ta which is used to aim the primary beam and to check if the rastering is correct. The second standard is ZnS which is used to aim the electron beam such that it is coincident with the primary beam.

The samples are then sputtered one at a time and the output of the machine is fed directly into a computer. The output is in the form of the number of counts of a species versus the sputtering time. The conversion of counts to concentration of tracer $\overline{C}_{18}(t_s)$ at a time t_s is given by :

$$\overline{C}_{18}(t_s) = \frac{h_{18}(t_s) - O\text{-}18esd}{(h_{18}(t_s) - O\text{-}18ESD)+(h_{16}(t_s) - O16ESD)} \quad ...(4.1)$$

where $h_{18}(t_s)$ and $h_{16}(t_s)$ are the counts of O-18 and O-16 at a sputtering time t_s. O-18ESD and O-16ESD are the ESD values of O-18 and O-16 measured by shutting off the primary beam. The sputtering time is converted to sputtering depth by measuring the depth of the crater by a profilometer and dividing it by the total time under the primary beam giving the sputtering rate

72

$\dot{S}$ such that:

$$Y_s = \dot{S} t_s \qquad \ldots(4.2)$$

where Y_s is the sputtered depth corresponding to the sputtering time t_s.

CHAPTER 5

RESULTS AND DISCUSSION

5.1 Reasons for choosing the alloy and technique

The theoretical modelling of the oxidation process of the FeCrAl-Zr alloy was done on the assumption that the oxide growth is planar, i.e., the oxide metal interface is sharp. Smialek studied the microstructure of the oxide formed on the same alloy. He found that at 1100 $^{\circ}$C, the oxide formed had closely packed polycrystalline grains and the oxide-metal interface was reasonably planar, at least for long oxidation times. At 1100 $^{\circ}$C there were very few pores observed in the oxide. Reddy [15] used the double oxidation technique on a NiCrAl alloy and concluded that the oxide was inward growing with the mechanism being oxygen grain boundary transport. There was no reason to beleive that the behaviour of FeCrAl-Zr alloy would be drastically different. So the FeCrAl-Zr alloy seemed like a good alloy to apply the double oxidation technique. Cawley [16] used

the double oxidation technique very successfully on Si and SiC. He used the SIMS to obtain the tracer concentration profile. He was able to experimentally obtain a sharp oxide interface as the oxygen signal in the SIMS fell down rapidly at the interface. He was also successful in determining the diffusion coefficients of oxygen from the observed concentration profile. His success was inspirational in choosing the double oxidation technique and SIMS for these experiments.

5.2 Lacey growth

When the tracer concentration profile in the oxide on a FeCrAl-Zr sample was obtained, it differed from the profiles obtained by Reddy on his NiCrAl-Zr samples. To try to interpret the difference the oxide was looked at under the SEM.* The microstructure as shown in Figure 18 varied drastically from that observed by Smialek on the same alloy. The sample had been polished by 3 micron diamond paste, annealed in vacuum at 1100 $^{\circ}$C for 30 minutes and oxidised for 40 hours at 1100 $^{\circ}$C.

----

* Courtsey J.Smialek and J.Cawley at NASA Lewis and M.Occhionero at Case Western Reserve University.
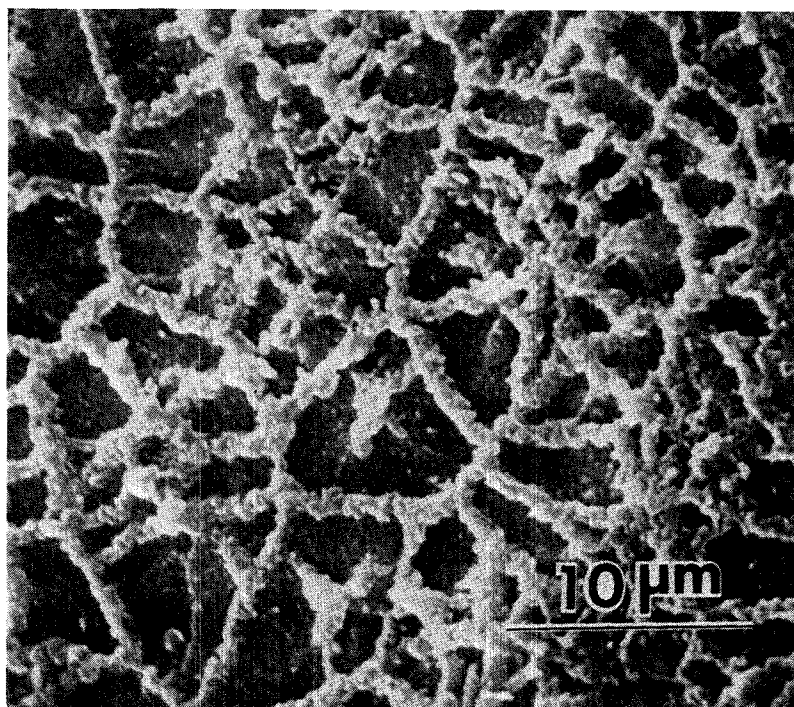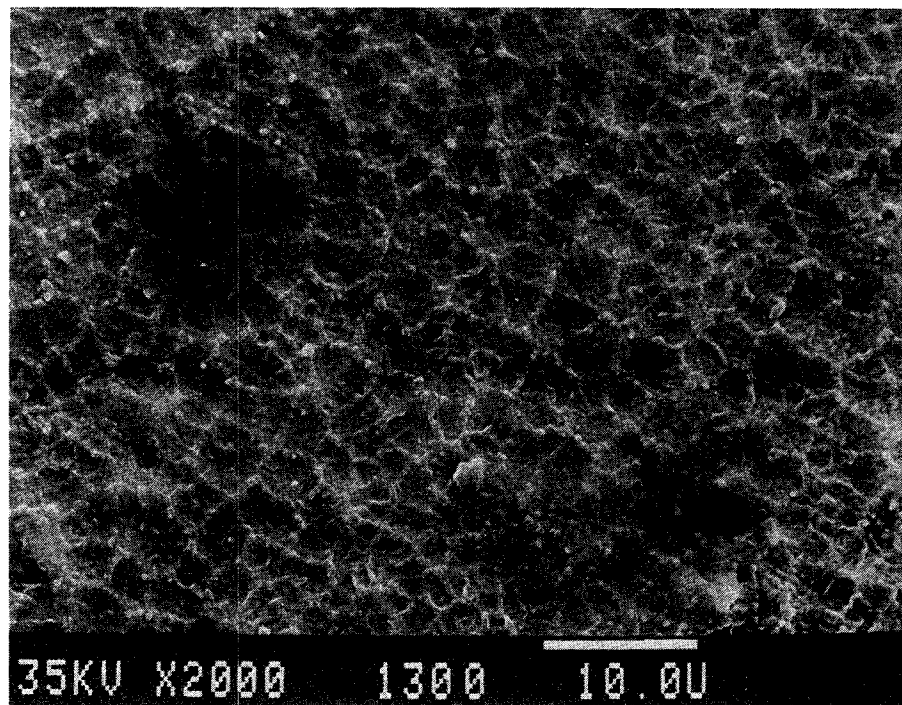
75

FIGURE 18 – Top view of the oxide at the gas-oxide interface.
The sample has been polished to a 3 micron
diamond paste finish, annealed in vacuum for 30
minutes at $1100^{\circ}C$ followed by a 40 hour oxidation
at $1100^{\circ}C$.

Instead of a compact polycrystalline scale, a lacey
structure of about 2 micron wide ridges was
observed at the oxide-gas interface. This shows
that the oxide growth is not planar.

To understand this difference in
microstructure a systematic study was undertaken.
The effect of three variables on the micro-
structure was studied: the oxidation time, the
surface finish of the sample and the time of vacuum
anneal. The vacuum anneal is done before the
oxidation to remove the polishing damage.

The development of the oxide microstructure
with time is shown in Figure 19. The alloy is
polished to a 1 micron diamond paste finish and
oxidized at 1100 ^{o}C for times of 3 hours, 10 hours,
20 hours and 36 hours , 25 minutes. The lacey
structure at the oxide-gas interface is evident at
least for the shorter oxidation times. The ridges
form a network of cells and the average cell size
seems to decrease with time. The average cell size
decreased from about 5 microns at 3 hours to about
3 microns at 10 hours and goes down to about 1.5
microns at 20 hours. At 36 hours and 25 minutes,

77

35KV X2000   1300   10.0U

19 a) 3 hour oxidation at 1100°C.

35KV X2000   1100   10.0U
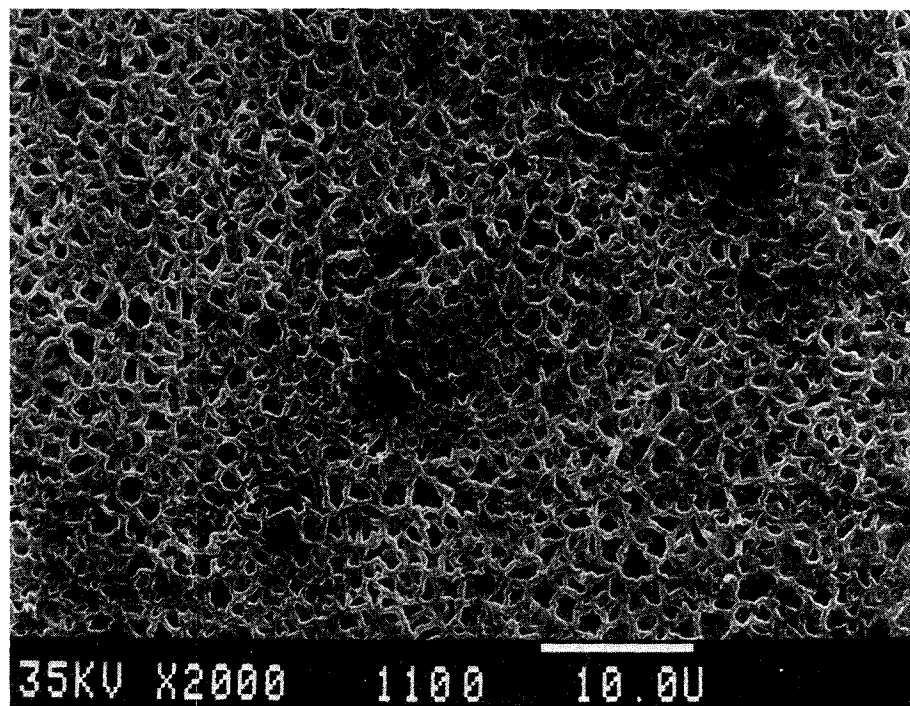
19 b) 10 hour oxidation at 1100°C.

35KV X2000   9000   10.0U
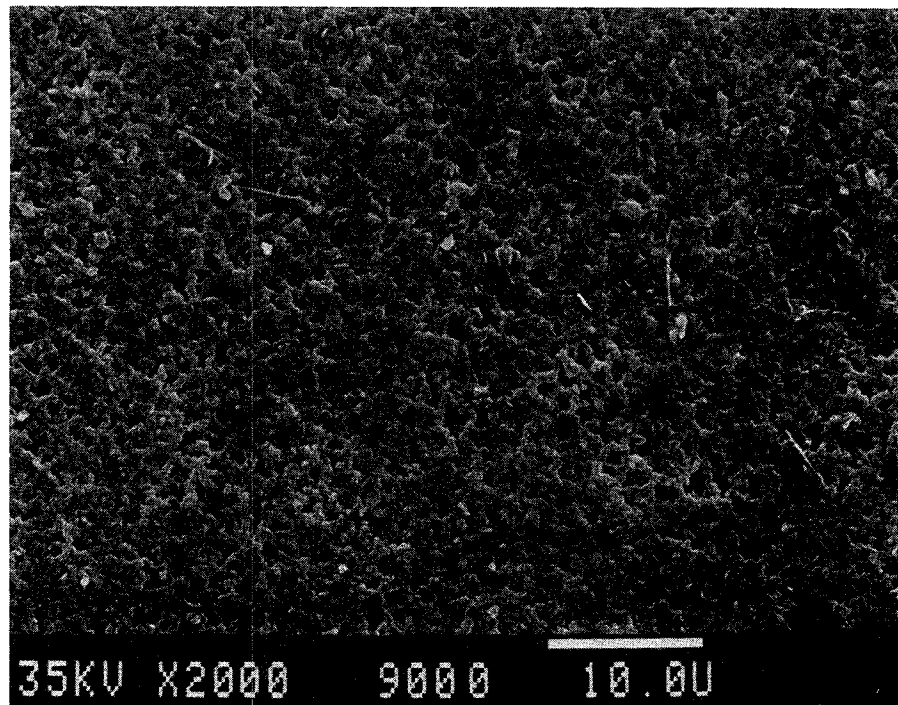
19 c) 20 hour oxidation at 1100°C.

35KV X2000   1400   10.0U
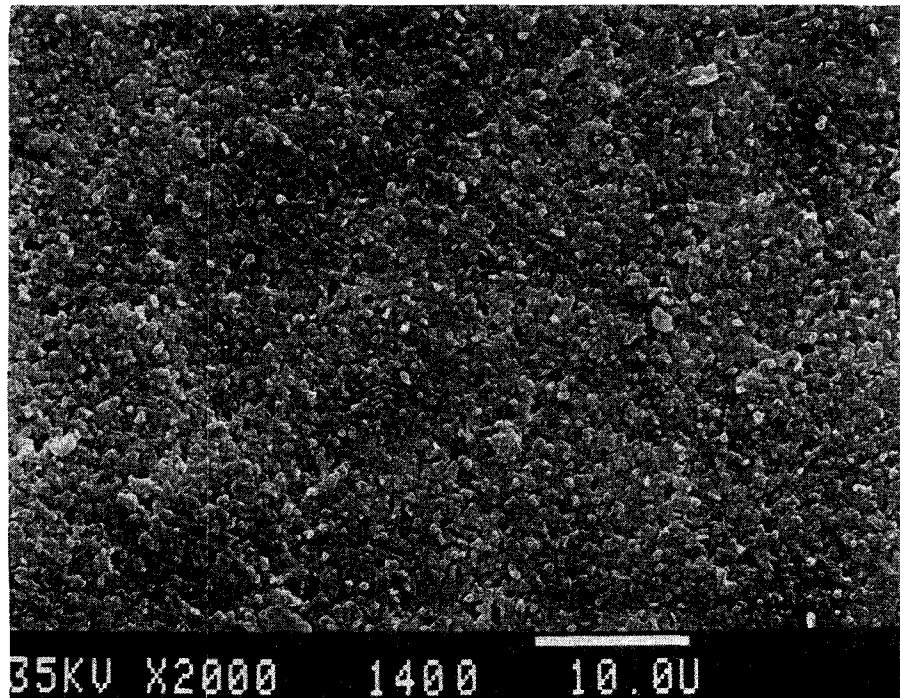
19 d) 36 hours, 25 minutes oxidation at 1100°C.

FIGURE 19 – Changes in microstructure of oxide at gas-
oxide interface with increasing oxidation
time. The samples have been polished to a
1 micron diamond paste finish.

the lacey structure cannot be seen and the
microstructure looks like that reported by Smialek.
So if only the long time microstructure was
examined it would seem to be a planar scale and
would encourage the application of the model to
derive quantitative information. However, such a
procedure would lead to errors as the oxide did not
start off looking that way and at least the initial
period of oxidation did not lead to a planar
oxide growth.

A detailed description of the oxidation
mechanism leading to the lacey structure will not
be attempted here. However it is important to note
that the outward aluminum diffusion must occur to
change the microstructure at the gas-oxide
interface. So at least for oxidation up to 20
hours, the oxide is not completely inward growing.
Hindam and Smeltzer [49], observed lace on Al_2O_3
scales grown on NiAl. They explained this
occurence by stating that the initial oxide formed
was $\gamma-Al_2O_3$ by inward oxygen diffusion. The scale
then went through a to tranformation accompanied by
a 14% reduction in volume. The α -alumina formed
was for most part oriented. However, this volume

reduction gave rise to some faulted oxide regions. The scale was thus a combination of oriented alumina and misoriented oxide which provided the path for combined inward oxygen and outward aluminium diffusion. This gave rise to ridges at the gas - oxide and the oxide-metal interface corresponding to misoriented oxide grains. However, this does not explain why the cell size of the lacey structure should decrease with time as the transformation occurs only once.

Hindam and Smeltzer observed that the structure of lace itself can be a function of the alloy grain orientation and can be vary drastically over two alloy grains in the same sample. Doychak [50] also observed a grain orientation dependency of the lacey structure during his study of NiAl oxidation. Work is presently being done by Smialek at NASA to understand the occurence of lace. The dependency of lace on the alloy grain orientation raises the question whether the observed decrease in cell size with time is real or an artifact because the four samples were so chosen that the alloy grain orientation led to a decreasing cell size. Though this is a possibility, the odds

83

against it are high.

Figure 19b) and Figure 20 show the effect of
surface finish on the lacey structure. The sample
in figure 20 has been polished by a 600 grit
polishing paper while the sample in Figure 19b) has
been polished by 1 micron diamond paste. Both the
samples have been oxidised for 10 hours at 1100°
C. No dramatic difference is observed in the lacey
structure which suggests that surface finsh may not
play a big role in lace formation.

The effect of the vacuum anneal on the lacey
structure can be seen by studying Figure 19b) and
Figure 21. The sample in Figure 19b) has not been
treated to the vacuum anneal while the sample in
Figure 21 has been annealed in vacuum for 30
minutes at 1100° C. The sample with no vacuum
anneal shows the lacey structure as a network of
cells with the average cell size around 3 microns.
However the structure of the sample with vacuum
anneal looks drastically different. The lace takes
up a spider like form with a nucleus and the lace
spreading in radial directions from it. This shows
up in certain areas of the oxide surface. Regions

35KV X2000   1000   10.0U
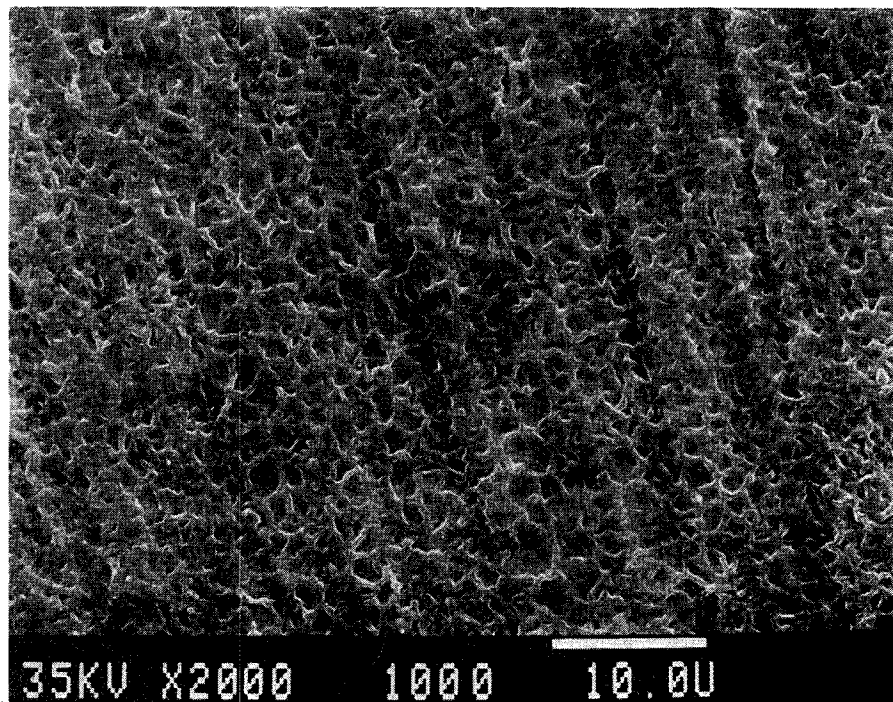
FIGURE 20 - Top view of oxide at the gas-oxide interface.
The sample has been polised by 600 grit polishing
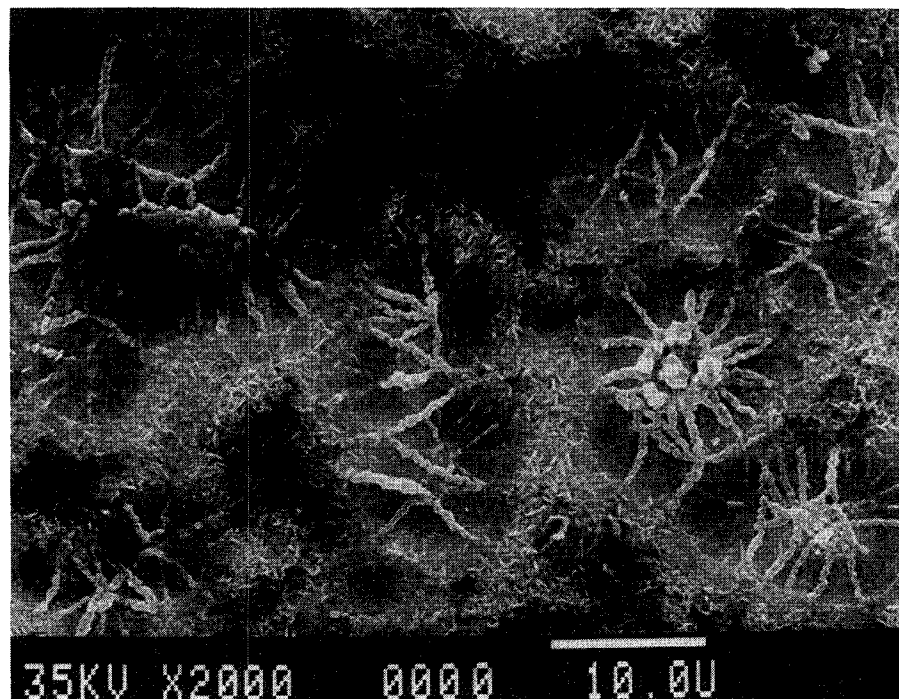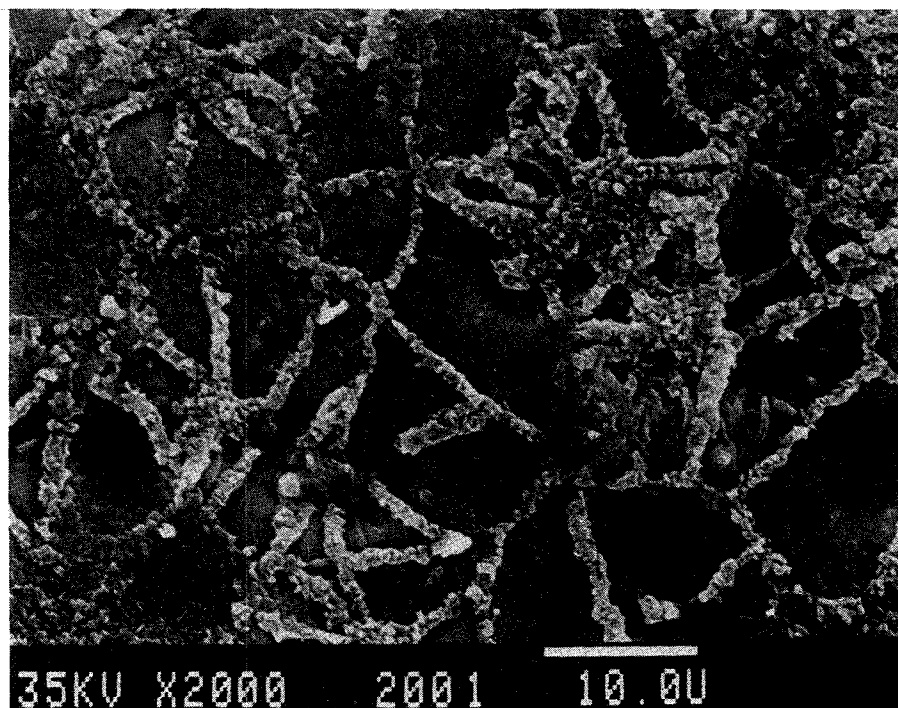paper and annealed for 10 hours at 1100°C.

FIGURE 21 - Top view of oxide at gas-oxide interface. The
sample has been polished to a 1 micron diamond
paste finish, annealed in vacuum for 30 minutes
at 1100°C followed by a 10 hour oxidation at
1100°C.

86

away from the lace covered areas have a needle like structure. A similar effect was observed at a higher temperature as shown in Figure 22. The sample in Figure 22a) was annealed for 30 minutes in vacuum at 1200° C while the sample in Figure 22b) had not been given any vacuum anneal. Both the samples were polished by a 1 micron diamond paste and oxidised for 10 hours at 1200° C. The formation of lace on the sample with vacuum anneal was much more dramatic. These observations suggest that vacuum annealing encourages the formation of lace at least at short oxidation times.

To study the effect of vacuum anneal on lacey structure for large oxidation times, two samples were oxidised at 1100° C for 50 hours. Both samples were annealed in vacuum for 30 minutes at 1100° C before oxidation. Figure 23 shows the microstructure of the oxide formed on the two samples. The sample in Figure 23a) has been polished with 1 micron diamond paste while the sample in Figure 23b) has been polished with 600 grit polishing paper. Both samples do not show lace. However, Figure 18 shows a dramatically different microstructure. The sample in Figure 18

35KV X2000 2001 10.0U

22 a) Vacuum anneal at 1100°C for 30 minutes prior
to oxidation.

35KV X2000   3000   10.0U
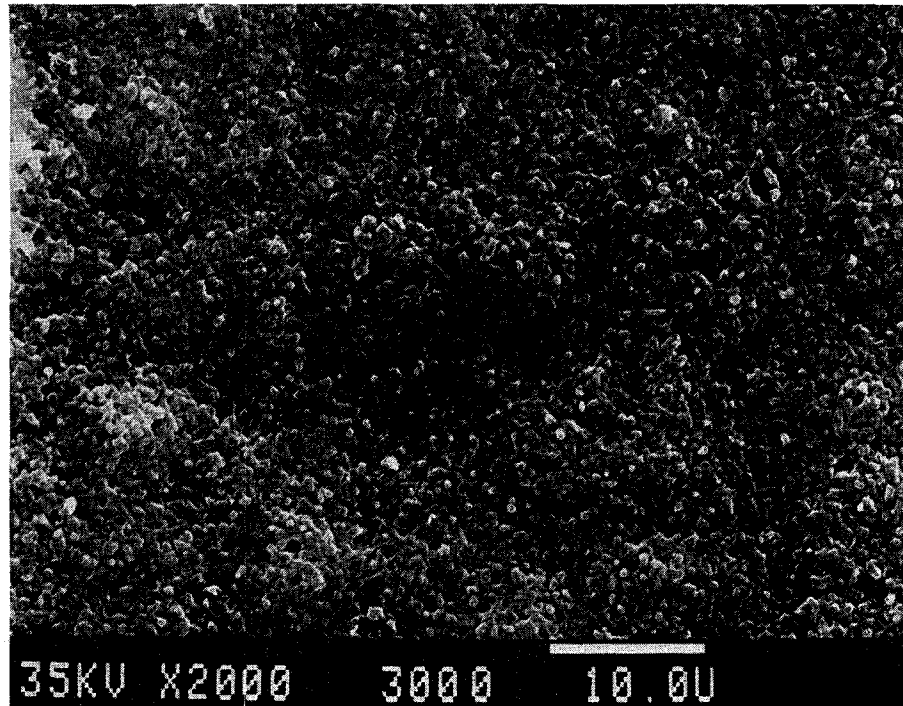
22 b) No vacuum anneal.

FIGURE 22 – Effect of vacuum anneal on oxide microstructure
at 1200°C. Both samples were polished to a 1
micron diamond paste finish and oxidised for 10
hours at 1200°C.

89

35KV X2000   4000   10.0U
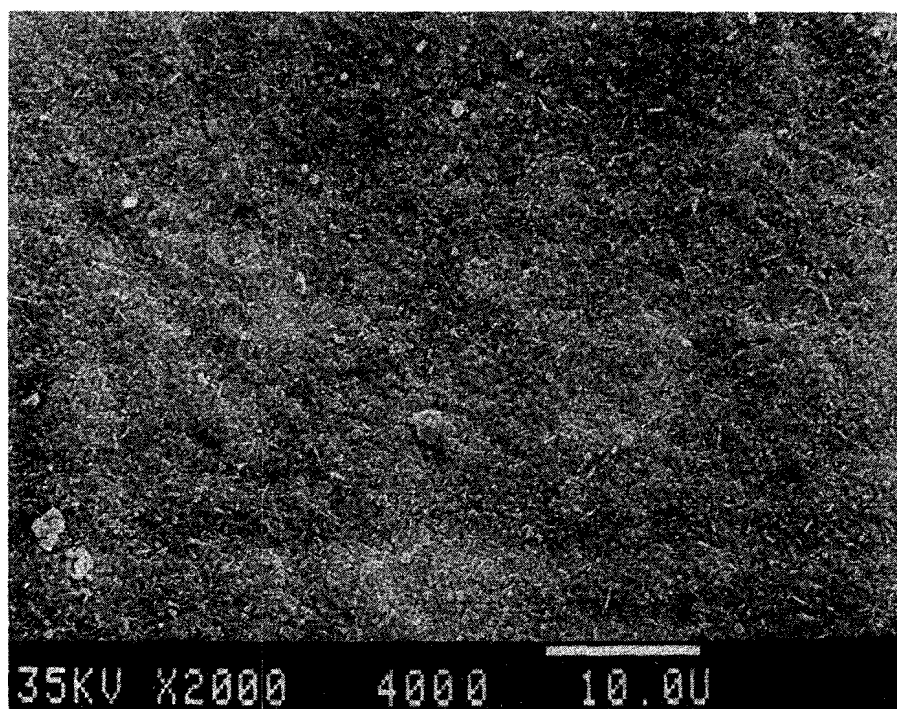
23 a) Microstructure of oxide at gas-oxide interface. The
      sample has been polished to a 1 micron diamond paste
      finish, annealed in vacuum for 30 minutes at 1100°C
      and oxidised for 50 hours at 1100°C.

35KV X2000 5000 10.0U
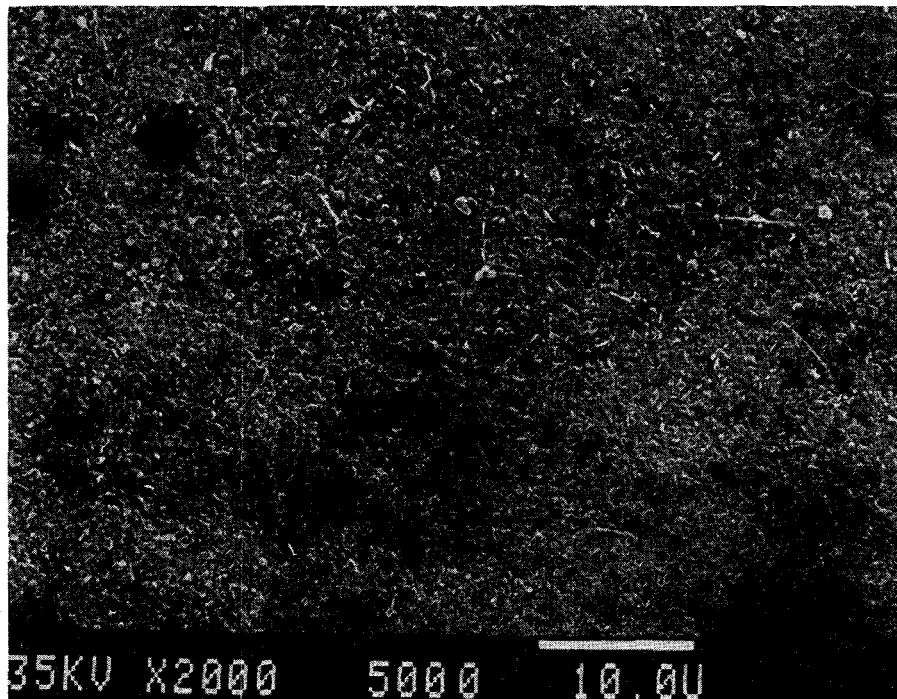
23 b) Microstructure of oxide at gas-oxide interface. The
sample has been polished by 600 grit polishing paper
annealed at 1100°C for 30 minutes and oxidised for
50 hours at 1100°C.

FIGURE 23 – Microstructure of oxide after long time oxidation.

91

has also been annealed in vacuum for 30 minutes at
1100°C after which it was oxidised for 40 hours at
1100°C. The specimen has been polished by 3 micron
diamond paste. This difference in micro-structure
may be due to different alloy grain orientation.

In conclusion, some of the facts about lace
and its structure are stated without an attempt to
explain the reason or the mechanism of structure
variation. Occurence of lace seems to be sensitive
to the vacuum anneal, at least at smaller times.
The vacuum anneal encourages the formation of lace.
The structure of the lace itself may vary from a
cell like structure in Figure 14b) to a spider like
structure in Figure 21. The cell size and shape of
the lace is sensitive to the alloy grain
orientation. The cell size of the lace may
decrease with time under isothermal oxidation. The
lace seems to have a radial texture, i.e., the
ridges seem to form radially from a nucleus.

The formation of lace and its structure does
not seem to be consistent and can vary from sample
to sample. Its erratic behaviour is a good reason
to refrain from speculating on its origin.

5.3 Sputter etching

An important point to consider is the quality of data obtained by SIMS. The question to be addressed is that if the alloy was to undergo planar oxidation in a manner described by the model, how accurate would be the tracer concentration profile obtained by SIMS. Data obtained by SIMS are in the form of ion counts versus sputtering time. Even though the counts are a strong function of the oxide matrix, the matrix dependency is removed by taking the ratio of O-18 counts to the total number of oxygen counts. However, the conversion of sputtering time to depth is valid only if the sputtering rate is a constant or a known function of time. The manner in which data is collected by SIMS is that the oxide is sputtered for a given length of time (1 sec in this case) and the counts reported is the average of the signal received over this period.

To understand how SIMS collects the data, consider a planar oxide with a true concentration profile $C(y)$ across it as shown in Figure 24. The data is collected by sputtering for a time Δt and

93
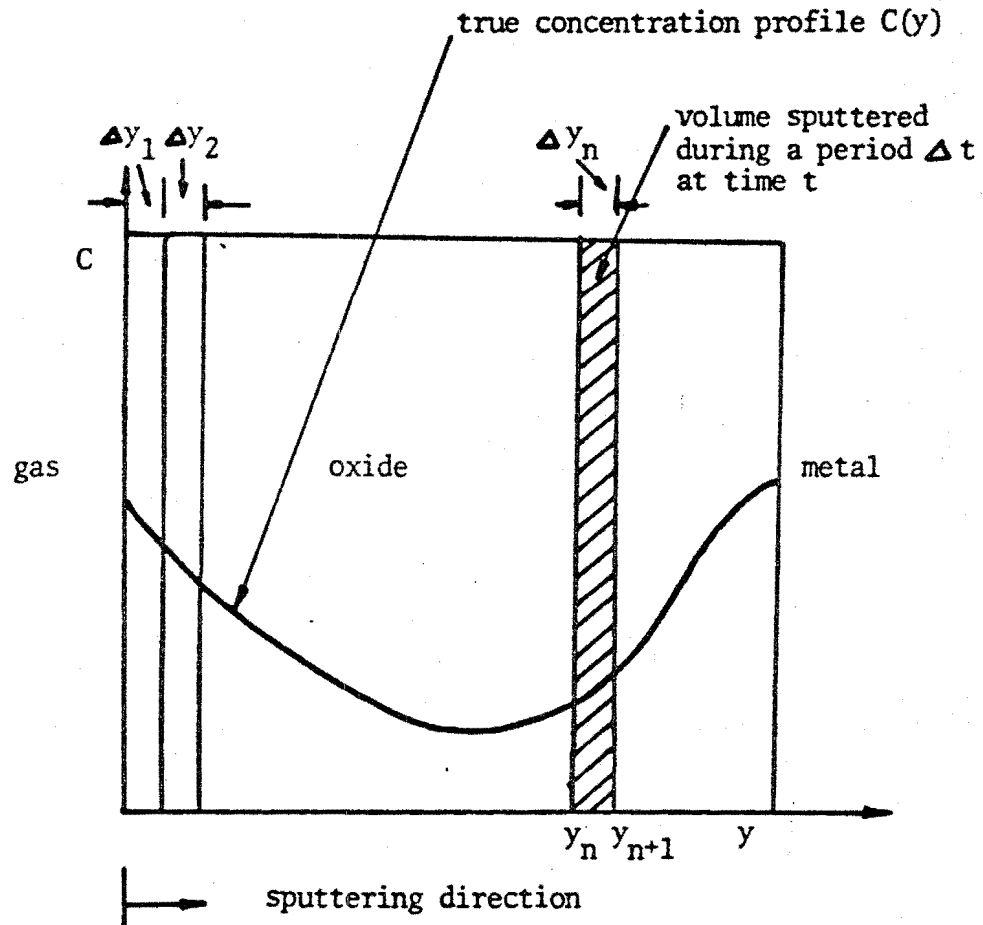
FIGURE 24 - Sputtering of oxide scale by SIMS.

94

averaging the number of counts collected over that
time period. Let Δy_1, Δy_2, ... Δy_n be the
thickness of oxide sputtered away after successive
sputterings of time Δt. The sputtered surface is
assumed to be flat. Then the concentraton reported
by SIMS at time t, C(t), is given by:

$$\overline{C}(t) = \overline{C}\left(\frac{y_n + y_{n+1}}{2}\right) = \frac{1}{\Delta y_n} \int_{y_n}^{y_{n+1}} C \, dy \qquad \ldots (5.1)$$

If the sputtering rate is constant , then all the
Δy's are the same.

Figure 25a) shows a step function concentraton
profile and Figure 25b) shows how the SIMS data
would appear for a constant sputtering rate when
the data in the form of counts versus sputtering
time is converted to a plot of concentration
versus distance. The profile obtained would be a
symmetric distortion of the true profile. However
it would be area preserving, i.e., the area under
the experimental concentration profile would be the
same as that under the true concentration profile.
Thus the mass balance ideas discussed in Chapter 2
would be valid and applicable to the observed
profile. However, if the sputtering rate is not
uniform, then the conversion of counts versus time
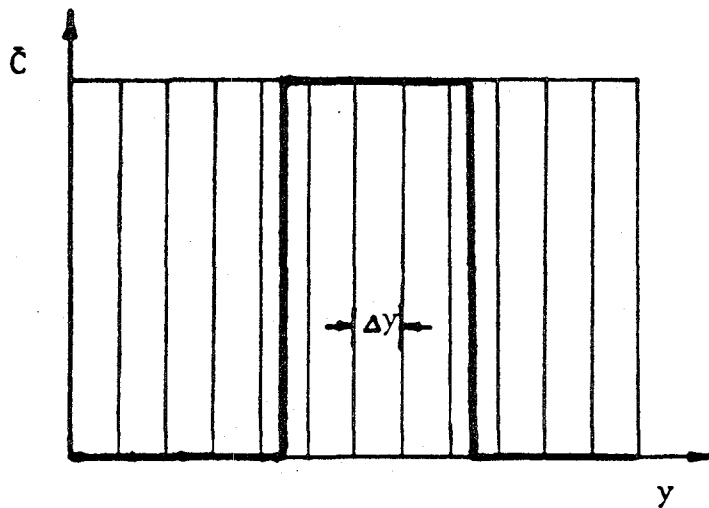
a)
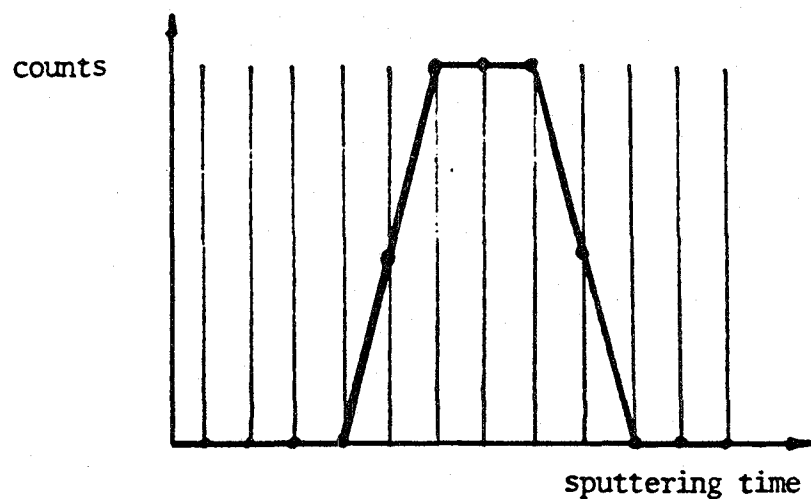
b)

FIGURE 25 - Distortion of concentration profile due to sputtering
by SIMS. a) Concentration profile. b) Output from SIMS.

to concentration versus distance by using Equation 4.2 would lead to an unsymmetrically distorted profile which would not be area preserving. In such a case the mass balance idea would not be applicable to the data.

A further complication occurs if the sputtered surface of the oxide is not planar but has instead a convoluted morphology as shown in Figure 26. Let $C(y)$ be the true concentration profile of the tracer in the oxide. In this case for a sputtering time of Δt information is being collected from a range of depths y_1 to y_2 and the reported concentration is the average of the concentration over this depth range weighted by the amount of material removed from a given depth. Let $dV(y)$ be the volume of oxide removed at depth y by sputtering for a time Δt. The average concentraton reported is given by:

$$\overline{C} = \frac{\int_{y_1}^{y_2} C(z)\ dV(z)}{\int_{y_1}^{y_2} dV(z)} \quad ...(5.2)$$

If the range of depths over which information is simultaneously received, is too large it may distort the concentration profile to an extent that obtaining quantitative information from it is

97
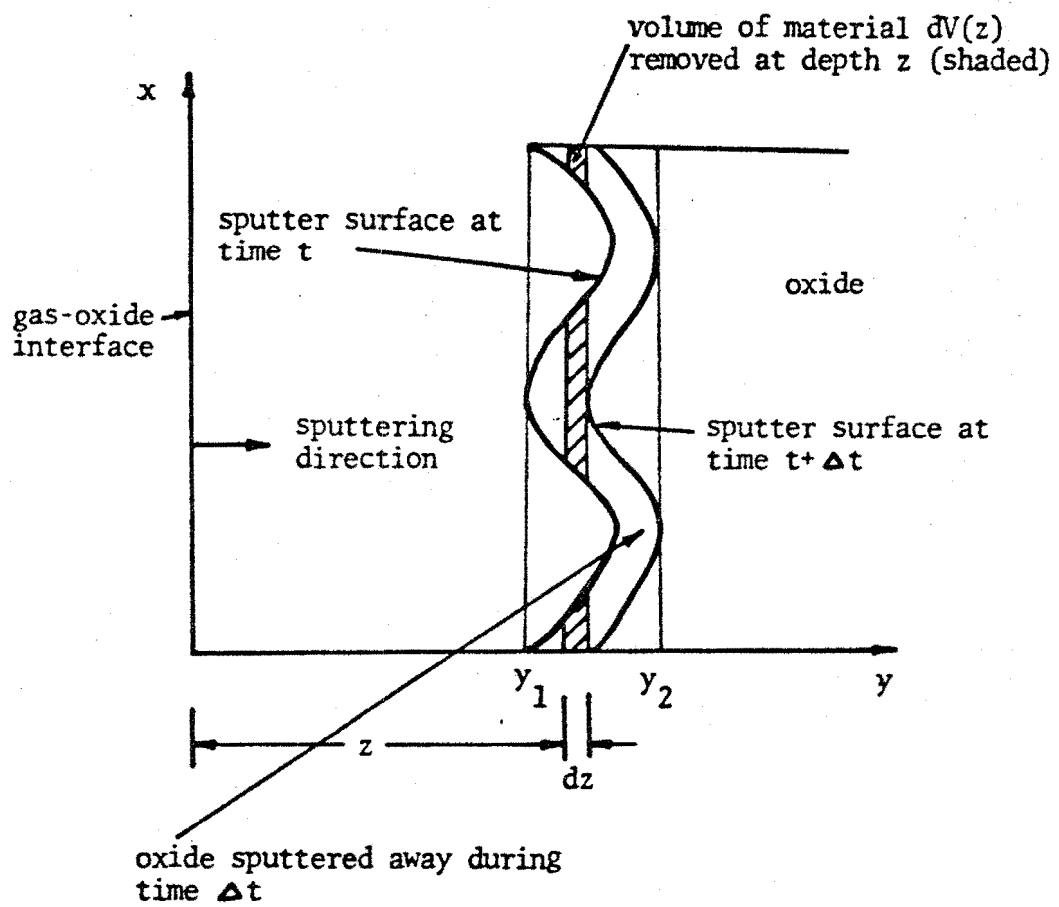
FIGURE 26 - Effect of non-uniform sputter surface.

impossible.

Another major problem faced when a sputter etching technique is used on a polycrystalline oxide is the phenomenon of preferential sputtering. The grain boundary region may sputter at a faster rate than the grains. The sputtering rate of the grains themselves may be a function of their orientation. This means that the range of depths over which the signal is collected will vary across the sputter surface. Figure 27a) shows the oxide scale being made up of 2 regions A and B where B sputters twice as fast as A. A could represent the grain while B could represent the grain boundary or alternately they could represent grains of fast and slow sputter orientation. Figure 27 shows the sputter surface after a sputtering time Δt. The reported concentration is the average of the concentraton measured over the shaded area in Figure 27b). This preferential sputter etching can also severely limit the resolution of the data.

5.4 SIMS data

gas
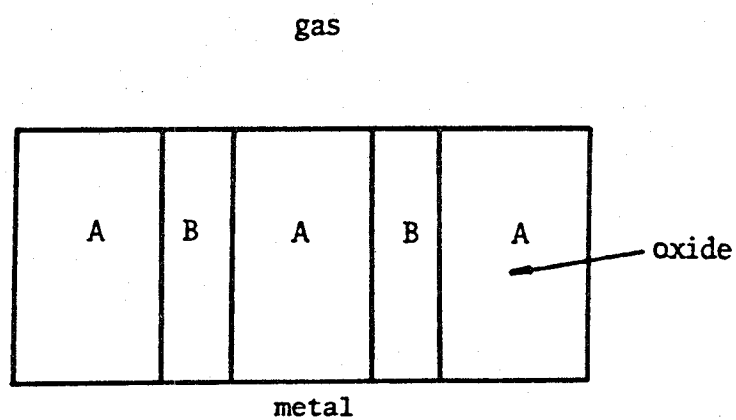
a)
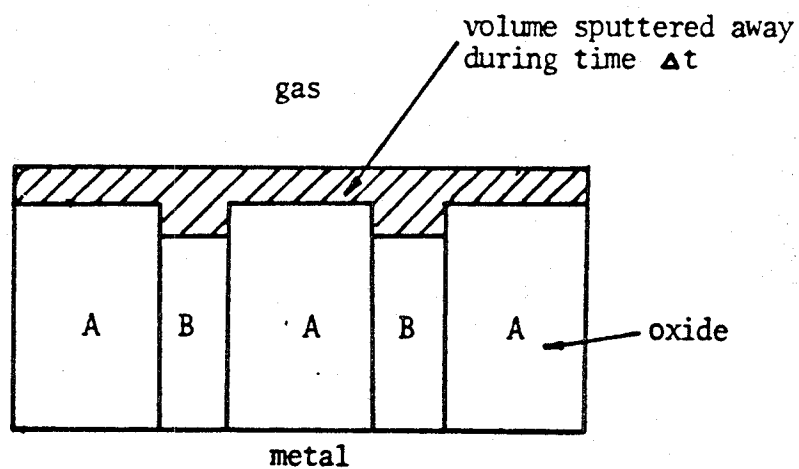
b)

FIGURE 27 - Preferential sputtering of oxide by SIMS.

Figure 28 shows the total counts of oxygen plotted as a function of normalised scale depth for a sample polished by 1 micron diamond paste and oxidised successively in air and O-18 tracer at 1100 ^{o}C for 20 hours and 16 hours, 25 minutes respectively. It is important to note that the oxygen counts drop off very gradually and there is no discontinuity indicating a sharp oxide-metal interface. This could be due to a combination of preferential sputtering and non planar oxide growth. Figure 29 shows a SEM picture of the same crater. The metal grains and the regions of oxide can be seen side by side as marked by M and O respectively. The lacey structure is evident in the oxide. The apparent tracer concentration profile of the same sample is plotted in Figure 30. If there was a sharp interface, the tracer concentration profile would have fallen off rapidly once the metal was reached. However, not only does the concentration profile at the interface not fall off steeply but it has a lesser slope than the near surface profile. This indicates that the problems of non planar oxide growth and preferential sputtering are too severe to apply our model to obtain quantitative data.

O-16 oxidation time=20 hours
O-18 oxidation time= 16 hours,25minutes
at 1100°C
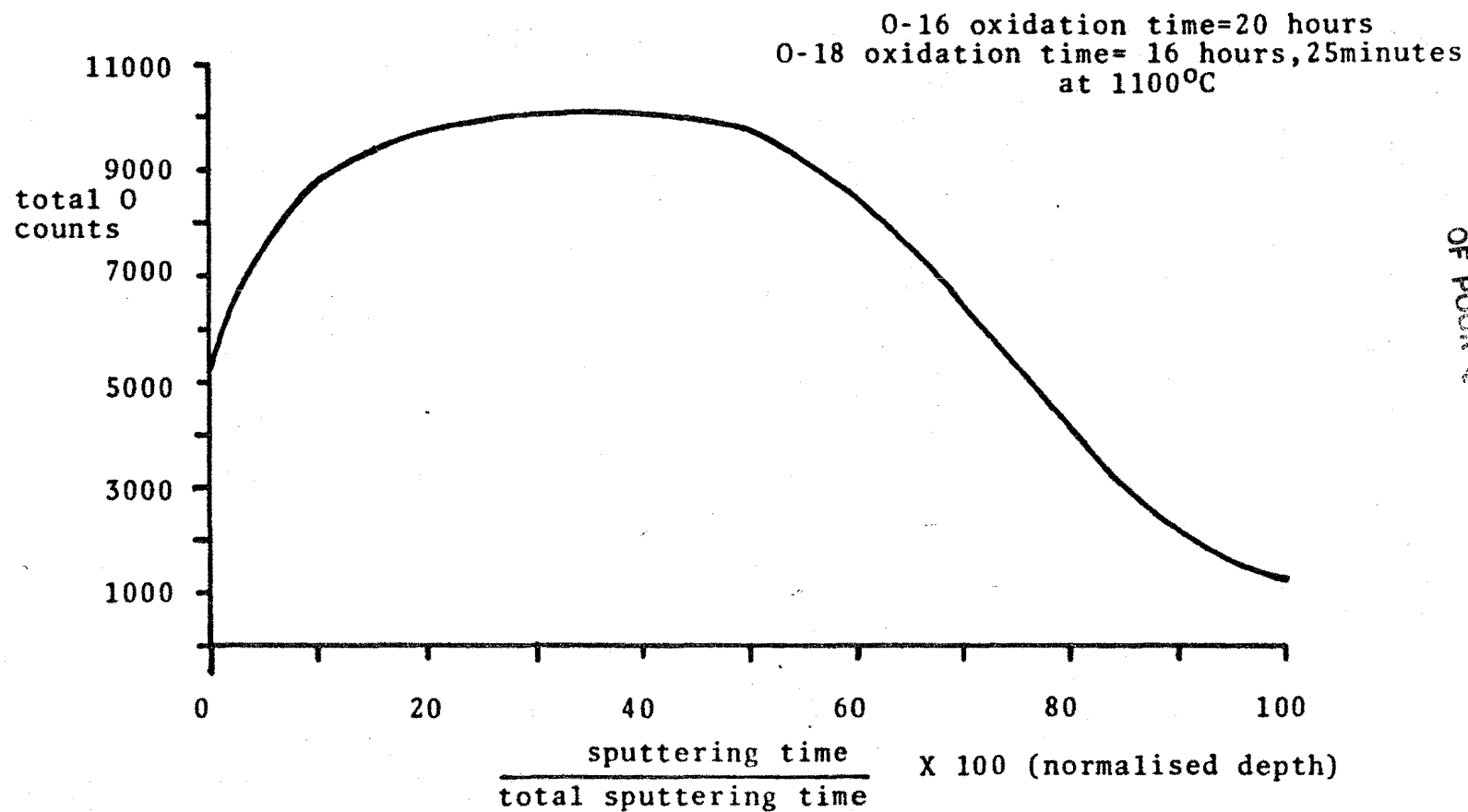
FIGURE 28 - Plot of total oxygen counts versus normalised depth.

$\dfrac{\text{sputtering time}}{\text{total sputtering time}}$ X 100 (normalised depth)

total O
counts
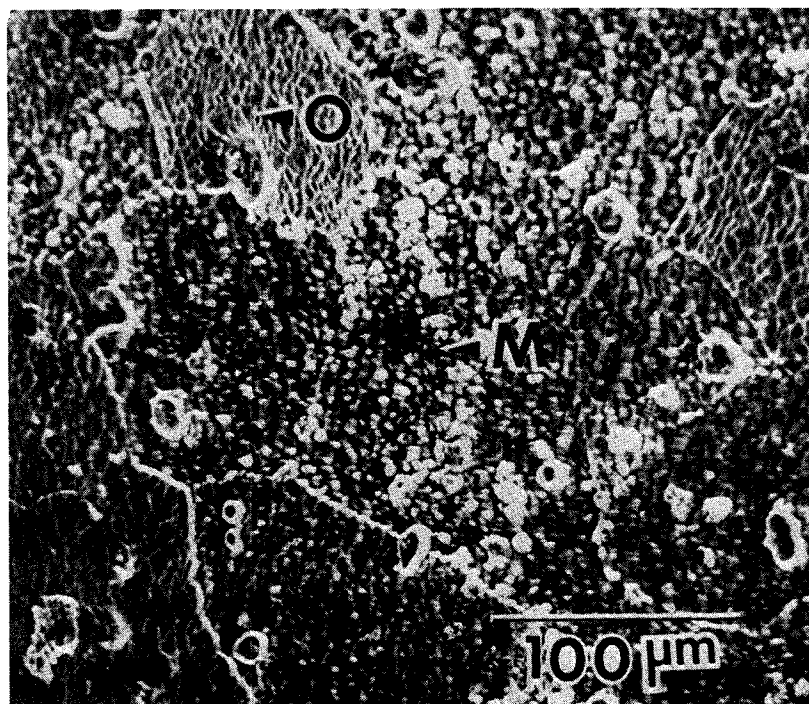
FIGURE 29 - Top view of the sputtered crater.

slope|A| > slope|B|

O-16 oxidation time=20 hours
O-18 oxidation time= 16 hours, 25 minutes
at 1100°C
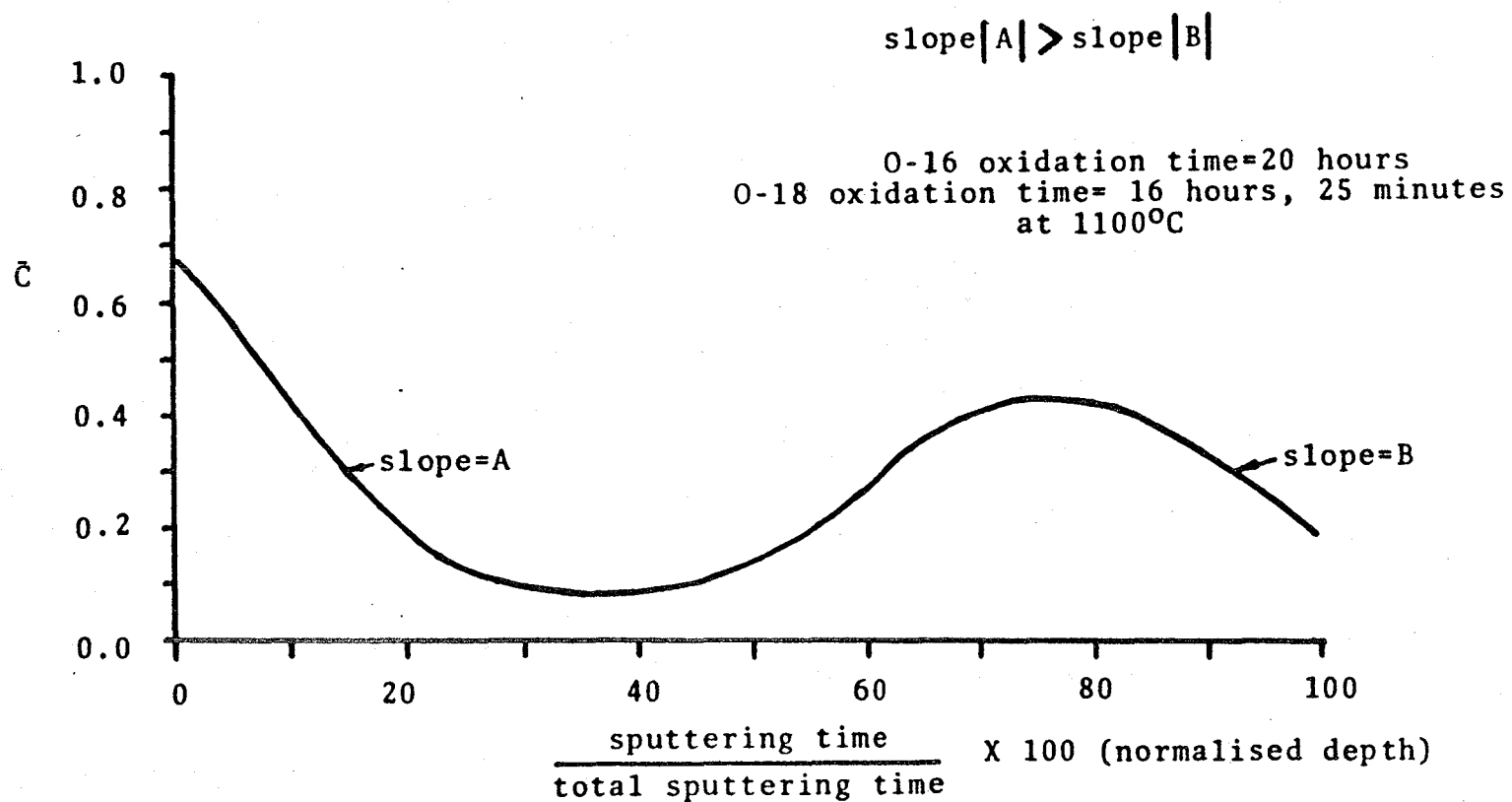
FIGURE 30 - Tracer concentration profile from SIMS

5.5 Conclusions

The aim of this study was to develop the double oxidation tracer technique. The thrust of the work was to come up with a method of analysis of the tracer concentration profile such that valuable information could be obtained from it.

The mass balance ideas developed can be used to deduce the oxidation mechanism from the tracer distribution in the oxide scale, if the oxide grows in a planar fashion. For all planar growing scales, if a true tracer concentration profile can be obtained, the fraction of inward and outward growth can be deduced by mass balance.

An effort was then made to develop an analysis which could be used to derive quantitative diffusion data from the tracer concentration profile. The specific diffusion problem of tracer distribution in a polycrystalline oxide scale growing by inward oxygen grain boundary diffusion with exchange was solved using a model based on the Oishi-Ichimura combined lattice and boundary diffusion model. For uniform grains across the

scale, unique profiles could be predicted using a combination of D, D_b and r. It was found that each parameter had a different effect on the profile. The model could be generalized to accomodate any grain size distribution obtained in a real oxide scale. Careful consideration was also given to the factors that could distort the data.

Having developed the analysis, it was tested on the FeCrAl-Zr alloy. Based on the extensive studies on NiCrAl alloys and long time oxidation studies on FeCrAl alloys by Smialek, the FeCrAl-Zr alloy was expected to oxidise in a planar fashion. However it was found that the oxidation behaviour of FeCrAl-Zr alloy was extremely unpredictable and the microstructure of the oxide varied from sample to sample and even within the sample. The formation and changes in the lacey structure at the gas-oxide interface suggested that outward cation transport also occured. So it was found that the FeCrAl-Zr alloy was not a good system to apply the model. The SIMS which had been very successfully used on amorphous materials led to preferential sputtering in the polycrystalline oxide scale and caused distortion of the tracer concentration

Profile. Thus no attempt was made to derive diffusion coefficients from the data obtained.

To exploit the analysis and quantitative modelling done in this thesis, it is necessasary to apply the double oxidation technique to systems with typically planar growing scales. There is also a need to improve the profiling techniques on polycrystalline scales using proton activation or SIMS having uniform sputter etching.

CHAPTER 6

SUGGESTIONS FOR FUTURE WORK

1. The realistic oxide microstructure could be incorporated in the computer program by treating the problem of varying grain size and shape across the oxide scale. For oxide scales having columnar grains, the exchange process could be treated as diffusion into a cylinder. The only modification required would be to substitute Equation 3.7 by the corresponding equation of diffusion of tracer into a cylinder having a constant surface concentration.

2. The presence of precipitates of a second phase with different oxygen diffusivity could be incorporated in the program by considering the variation of lattice diffusivity across the oxide scale.

3. The problem of combined inward oxygen tracer diffusion with exchange and outward aluminum diffusion could be addressed.

4. The amount of O-16 in the old oxide undergoing direct surface exchange with the gas during tracer oxidation can be calculated. This would lead to a

modification of the mass balance ideas. However the amount of O-16 involved in direct exchange with the gas is not very significant (Appendix B).

5. A system with an inherently planar growing oxide scale should be chosen to apply this model. The analysis techniques developed could be applied to the existing tracer concentration data on NiO by Atkinson et. al.[51] and NiCrAl-Zr by Reddy [15].

REFERENCES

1. P.G.Shewmon, Diffusion in Solids, McGraw Hill, N.Y. (1963)

2. J.B.Wagner, "Defects in Oxides", Am. Ceram. Soc. Bulletin 53, 224 (1974)

3. W.D.Kingery, "Plausible Concepts Necessary and Sufficient for Interpretation of Ceramic Grain Boundary Phenomenon: I", J. Am. Ceram. Soc., 57, 1 (1974)

4. W.D.Kingery, "Plausible Concepts Necessary and Sufficient for Interpretation of Ceramic Grain Boundary Phenomenon: II", J. Am. Ceram. Soc., 57, 22 (1974)

5. J.C.Fisher, "Calculation of Diffusion Penetration Curves for Surface and Grain Boundary Diffusion", J. Appl. Phys., 22, 74 (1951)

6. R.T.P.Whipple, "Concentration Countours in Grain Boundary Diffusion", Phil. Mag., 45, 1225 (1954)

7. H.S.Levine and C.J.MacCallum, "Grain Boundary and Lattice Diffusion in Polycrystalline Bodies", J. Appl. Phys., 31, 595 (1960)

8. A.D.LeClaire,"The Analysis of Grain Boundary Diffusion Measurements", Brit. J. Appl. Phys., 14, 351 (1960)

9. T.Suzuoka, "Exact Solution of Two Ideal Cases in Grain Boundary Diffusion - Problem and Application to Sectioning Methods", J. Phys. Soc. Jap., 19, 839 (1964)

10. G.Zaeschmar, "Theory of Diffusion in a Polycrystalline Material", J, Appl. Phys., 54 (5), 2281 (1983)

11. Y.Oishi and H.Ichimura, "Grain Boundary Enhanced Interdiffusion in Polycrystalline CaO - Stabilised Zirconia System", J. Chem. Phys., 71 (12), 5134 (1979)

12. Y.Oishi and W.D.Kingery, "Self Diffusion of Oxygen in Single Crystal and Polycrystalline Aluminum Oxide", J. Chem. Phys., $\underline{33}$, 480 (1960)

13. Y.Oishi, K.Ando and K.Matsuhiro, "Self Diffusion of Oxygen in Vapour Grown Single Crystal Alumina", Yogyo Kyoka Shi, $\underline{85}$, 522 (1977) Quoted in Ref.15

14. D.J.Reed and B.J.Weunsch, "Ion Probe Measurement of Oxygen Self Diffusion in Single Crystal Al_2O_3", J. Amer. Ceram. Soc., $\underline{63}$, 88 (1980)

15. K.P.R.Reddy, "Oxygen Diffusion in Close Packed Oxides", Ph.D. Thesis, Case Western Reserve University (1979)

16. J.Cawley, "Oxygen Diffusion in Alpha-Alumina", Ph.D. Thesis, Case Western Reserve University (1984)

17. R.E.Mistler and R.L.Coble, "Grain Boundary Diffusion and Boundary Widths in Metals and Ceramics", J. Appl. Phys., $\underline{45}$, 1507 (1974)

18 D.L.Johnson and L.Berrin, pp. 445-69 in Sintering and Related Phenomena, ed. by G.C.Kuczynski, N.A.Hooton and C.F.Gibbon, Gordon and Breach, N.Y. (1967) Quoted in Ref.15

19. P.A.Lessing and R.S.Gordon, "Creep in Polycrystalline Alumina Pure and Doped with Transition Metal Impurities", J. Mat. Sci., $\underline{12}$, 2291 (1977)

20. C.L.Angerman, "Long Term Oxidation of Superalloys", Oxid. Met., $\underline{5}$, 149 (1972)

21. C.S.Giggins and F.S.Pettit, "Oxidation of Ni-Cr-Al Alloys Between 1000 and $1200^{\circ}C$", J. Electro. Chem. Soc., $\underline{118}$, 1782 (1971)

22. J.L.Smialek and R.Gibala, "Structure of Transient Oxides Formed on NiCrAl Alloys", Metall. Trans. A, $\underline{14}$, 2143 (1983)

23. F.A.Golightly, G.C.Wood and F.H.Stott, "The Early Stages of Development of α-Al_2O_3 Scales on

FeCrAl and FeCrAl-Y Alloys at High Temperature",
Oxid. Met., _14_, 217 (1980)

24. H.M.Hindam and W.W.Smeltzer, "Application of
Auger Electron Spectroscopy and Inert Marker
Techniques to Determine Metal and Oxygen
Transport in Oxide Films on metals", Oxid. Met.
_14_, 337 (1980)

25. K.P.R.Reddy, J.L.Smialek and A.R.Cooper, "O-18
Tracer Studies of Al_2O_3 Scale Formation on
NiCrAl Alloys", Oxid. Met., _17_, 429 (1982)

26. F.A.Golightly, F.H.Scott and G.C.Wood, "The
Influence of Yttrium Addition on the Oxide Scale
Adhesion to an Iron Chromium Aluminium Alloy",
Oxid. Met. _10_, 163 (1976)

27. D.P.Whittle and J.Stringer, "Improvement in High
Temperature Oxidation Resistance by Addition of
Reactive Elements on Oxide Dispersons", Phil.
Trans. Of Royal Soc. Lon., _295_, 309 (1980)

28. D.Delaunay and A.H.Huntz, "Mechanism of
Adherence of Alumina Scale Developed during High
Temperature Oxidation of Fe-Ni-Al-Y alloys ", J.
Mat. Sci., _17_, 2027 (1982)

29. J.C.Pivin, D.Delauney, C.Roques, A.M.Huntz and
P.Lacombe, "Oxidation Mechanism of
Fe-Ni-20-25Cr-5Al Alloys – Influence of Small
Amounts of Yttrium on Oxidation Kinetics and
Oxide Adherence", Corr. Sci., _20_, 351 (1980)

30. D.Delauney, A.M.Huntz and P.Lacombe, "Mechanical
Stress Developed in High Temperature Resistant
Alloys During Isothermal and Cyclic Oxidation
Treatments: The Influence of Yttrium Additions
on Oxide Scale Adherence", Corr. Sci., _20_, 1109
(1980)

31. J.L.Smialek, "Microstructure Of Al_2O_3 Scales
Formed On NiCrAl Alloys", Ph.D. Thesis, Case
Western Reserve University (1981)

32. J.L.Smialek and R.Gibala, "Diffusion Process in
Al_2O_3 Scales. Void Growth, Grain Growth and
Scale Growth", High Temperature Corrosion,
NACE-6 274 (1983)

33. J.L.Smialek "Growth Kinetics and Micro Structure of Al_2O_3 Scale Formed on NiCrAl Alloys", conference on Oxidation Deposition and Hot Corrosion In Combustible Turbine Engines, NASA Lewis Research Center (1983)

34. D.G.Lees and J.M.Calvert "The Use of O-18 as a Tracer to Study the Growth Mechanisms of Oxide Scales", Corr. Sci. 16, 767 (1976)

35. J.S.Sheasby and J.D.Brown "The Use Of SIMS to Investigate the Incorporaton of Oxygen in CoO Scales", Oxid. Met, 12, 405 (1978)

36. A.M.Pritchard, N.E.W.Hartley, J.F.Singleton and A.E. Truswell "Oxygen 18 and Deutrium profiling in Thick Films on Fe-9% Cr Alloys by 3MeV Nuclear Microprobe", Corr. Sci., 20, 1 (1980)

37. C.Gleave, J.M.Calvert, D.G.Lees and P.C.Rowlads, "A Study of the Mechanisms of Corrosion of Some Ferritic Steels in High Pressure Carbon Dioxide with aid of Oxygen-18 as a Tracer. I. Low Silicon Mild Steel", Proc. Roy. Soc. Lond., 379, 409 (1982).

38. C.Gleave, J.M.Calvert, D.G.Lees and P.C.Rowlands "A Study of the Mechanism of Corroson of Some Ferritic Steels in High Pressure Carbon dioxide With the aid of Oxygen-18 as a tracer Ii. High Silicon Mild Steel. Proc. Roy. Soc. Lond., 379, 429 (1982)

39. A.W.Czanderna, Methods and Phenomena 1. Methods of Surface Analysis, Elsevier Scientific Publising, N.Y. (1975)

40. P.Williams, "Anomolous Sputter Yields due to Cascade Mixing", Appl. Phys. Lett., 36, 9 (1980).

41. Z.L.Liau, B.Y.Tsau and J.W.Mayer, "Influence of Atomic Mixing and Preferential Sputtering on Depth Profiles and Interfaces", J. Vac. Sci .Technol. 16, 121 (1979)

42. H.W.Werner and A.E.Morgan, "Charging of Insulators by Ion Bombardment and Its minimization for secondary ion mass spectroscopy

(SIMS) measurements", J. Appl. Phys. <u>47</u>, 1232 (1976)

43. J.R.Manning, <u>Diffusion Kinetics for Atoms in Crystals</u>, D. Von Nostrand Company Inc, NJ (1968)

44. J.Crank, <u>The Mathematics of Diffusion</u>, Cleardon Press, Oxford (1956)

45. M.L.James, G.M.Smith, J.C.wolford, <u>Analog and Digital Computer Methods in Engineerng Analysis</u>", International Text Book co, Scranton Pa (1964)

46. D.R.Gaskell, <u>Introduction to Metallurgical Thermodnamics</u>, McGraw Hill, N.Y. (1981)

47. R.Hultgren, <u>Selected Values of Thermodynamics Properties of Metals and Alloys</u>, John Wiley, N.Y. (1963)

48. K.P.D.Lagerlof, "Deformation and Diffusion in Sapphire (Al_2O_3)", Ph.D. Thesis, Case Western Reserve University (1984)

49. H.M.Hindman and W.W.Smeltzer, "Growth and Microstructure of Al_2O_3 on NiAl", J. Electrochem. Soc., <u>127</u>, 1630 (1980)

50. J.Doychak, Ph.D.Thesis in progress, Case Western Reserve University (1984)

51. A.Atkinson, R.I.Taylor and P.D.Goode, "Transport Processes in the Oxidation of Ni Studied Using Tracers in Growing NiO Scales", Oxid. Met. , <u>13</u>, 519 (1979)

APPENDIX A

Listing of the Computer Program


```
        dimension c(40),ci(40),ca(40),ti(40),csrain(40)
        open (unit=1,status='old',name='fplf.dat')
        READ(1,*)concint
        read(1,*)dop,sc
        READ(1,*)W3
        read(1,*)tstop,temp,tau,dl,sbwd,okp
        READ(1,*)W4
        read(1,*)ssize,dsb
        open(unit=2,status='new',name='lpfl.obj')
        open(unit=3,status='new',name='srate.obj')
        open(unit=4,status='new',name='sbc.obj')
        write(2,3)
3       FORMAT(5X,6HTEMP, ,10HO-18TIME, ,8HO-16TIME)
        write(2,4)temp,tstop,tau
4       format(4X,F6.0,3x,f6.0,4X,f6.0)
        write(2,8)
8       FORMAT(5X,14HGRAINSIZE(M), ,25HGB-DIFF
     *  COEFF(M**2/SEC), ,
     *  21HLDIFF COEFF(M**2/SEC),5x,5hsbwd )
        write(2,9)ssize,dsb,dl,sbwd
9       format(5x,e11.3,5x,e11.3,13X,E11.3,10x,e11.3)
        write(2,10)
10      format(3X,5H time,4x,1h1,5x,1h2,5x,
     *  1h4,5x,1h6,5x,1h8,5x,2h10,4x,
     *  2h12,4x,2h14,4x,2h16,4x,2h18,4x,2h20)
        READ(1,*)W5
        read(1,*)tinc,dtpr
        t=0.
        tprint=dtpr
        do 85 k=1,20
        ti(k)=0.0
85      continue
        c(1)=0.5
        do 11 j=2,21
        c(j)=0.0
11      continue
        do 700 j=1,20
        csrain(j)=0.0
700     continue
        tsrate=((20.0/19.0)**2.0)*tau
        nscount=20
        xscale=20.0
```

```
            delty=((okp*tau)**0.5)/19.0
26          t=t+tinc
            alpha=dsb*dop/(sc*temp*((okp*(T+tau))**0.5))
            a=4*dl/(ssize*sbwd)
            B=((3.14/GSIZE)**2.)*DL*T
            var=0.
            DO 12 N4=1,20
            var=var+exp(-b*(N4**2.))
            VAR4=EXP(-B*(N4**2))
            IF(VAR4/VAR.LE.0.01)GO TO 100
12          continue
100         N4=1
            beta=a*var
            x=(dsb/(delty**2.))-(alpha/(2.*delty))
            y=(1./tinc)-(2*dsb/(delty**2.))-beta
            z=(dsb/(delty**2.))+(alpha/(2.*delty))
            do 16 J=2,nscount
16          ci(J)=tinc*(x*c(J+1)+y*c(J)
     *      +z*c(J-1)+beta*csrain(J))
            ci(1)=1.0*concint
            ci(40)=0.0
            do 35 k=1,nscount
            if(ci(k).le.0.0)go to 35
            ti(k)=ti(k)+tinc
35          continue
            if(t-tprint)20,17,17
17          continue
            write(4,800)t,ci(2),ci(8),ci(16),
     *      ci(20),ci(21),ci(22),ci(23),
     *      ci(24),ci(25),ci(26),ci(27),ci(28)
800         format(1x,f7.0,12f5.2)
            do 80 J=1,20
            b=((3.14/ssize)**2.)*dl*ti(J)
            call expcal(b,vop)
            ca(J)=(1-((6./(3.14**2.))*vop))*
     *      (ci(J)-csrain(J))+csrain(J)
            ca(J)=(((ssize/2.0)**3.)*
     *      ca(J)+1.5*((ssize/2.)**2.)*
     *      sbwd*ci(J))/(((ssize/2.)+(sbwd/2.))**3.)
80          continue
            write(2,18)t,ca(1),ca(2),ca(4),
     *      ca(6),ca(8),ca(10),ca(12),ca(14),
     *      ca(16),ca(18),ca(20)
18          format(1X,F7.0,11F6.2)
            tprint=tprint+dtpr
20          if(t-tstop)515,21,21
21          do 90 J=1,nscount
            b=((3.14/ssize)**2.)*dl*ti(J)
            call expcal(b,vop)
```

116

```
         ca(j)=(1-((6./(3.14**2.))*vop))*
      *  (ci(j)-csrain(j))+csrain(j)
         ca(J)=(((ssize/2.0)**3.)*
      *  ca(j)+1.5*((ssize/2.)**2.)*
      *  sbwd*ci(j))/(((ssize/2.)+(sbwd/2.))**3.)
90       continue
         write(2,30)t,ca(1),ca(2),ca(4),
      *  ca(6),ca(8),ca(10),ca(12),ca(14),
      *  ca(16),ca(18),CA(20)
30       FORMAT(1X,F7.0,11F6.2)
         write(2,150)ci(20)
150      format(///f7.2)
         area1=0.0
         do 600 n=1,19
         areai=(ca(n)+ca(n+1))/2.0
         area1=area1+areai
600      continue
         area2=0.0
         nsc=nscount-1
         do 680 J=20,nsc
         areaJ=1.0-((ca(n)+ca(n+1))/2.0)
         area2=area2+areaJ
680      continue
         xinc=(area1-area2)/(1.0-ci(nscount))
         xscale=xscale+xinc
         write(3,610)t,xscale,xinc,
      *  ca(21),ca(22),ca(23),ca(24),ca(25),
      *  ca(26),ca(27),ca(28),ca(29)
610      format(1x,f7.0,2x,f6.2,1x,f5.2,1x,9f6.2)
         stop
515      continue
         tcounter=t+tau
         if(tcounter-tsrate)520,530,530
530      continue
         do 580 J=1,nscount
         b=((3.14/ssize)**2.)*dl*ti(j)
         call expcal(b,vop)
         ca(j)=(1-((6./(3.14**2.))*vop))*
      *  (ci(j)-csrain(j))+csrain(j)
         ca(j)=(((ssize/2.0)**3.)*ca(j)
      *  +1.5*((ssize/2.)**2.)*
      *  sbwd*ci(j))/(((ssize/2.)+(sbwd/2.))**3.)
580      continue
         write(2,640)t,ca(1),ca(2),ca(4),
      *  ca(6),ca(8),ca(10),ca(12),ca(14)
      *  ,ca(16),ca(18),ca(20)
640      format(1x,f7.0,11f6.2)
         area1=0.0
         do 500 n=1,19
```

```
        areai=(ca(n)+ca(n+1))/2.0
        area1=area1+areai
500     continue
        area2=0.0
        jnsc=nscount-1
        do 670 j=20,jnsc
        areaj=1.0-((ca(n)+ca(n+1))/2.0)
        area2=area2+areaj
670     continue
        xinc=(area1-area2)/(1.0-ci(nscount))
        xscale=xscale+xinc
        write(3,510)t,xscale,xinc,
     *  ca(21),ca(22),ca(23),ca(24),ca(25),
     *  ca(26),ca(27),ca(28),ca(29)
510     format(1x,f7.0,2x,f6.2,1x,f5.2,1x,9f6.2)
        tsrate=((tau**0.5)/19.0+(tsrate**0.5))**2.0
        csrain(nscount+1)=ci(nscount)
        ci(nscount+1)=ci(nscount)
        nscount=nscount+1
520     go to 24
24      DO 25 K=1,40
        c(k)=ci(k)
25      continue
        go to 26
        end
        subroutine expcal(b1,out)
        out=0.0
        do 60 n=1,20
        n2=n**2
        out=out+(exp(-b1*n2)/n2)
        var2=(out-(exp(-b1*n2)/n2))/out
        if(var2.st.0.99)go to 70
60      continue
70      n=1
        end
```
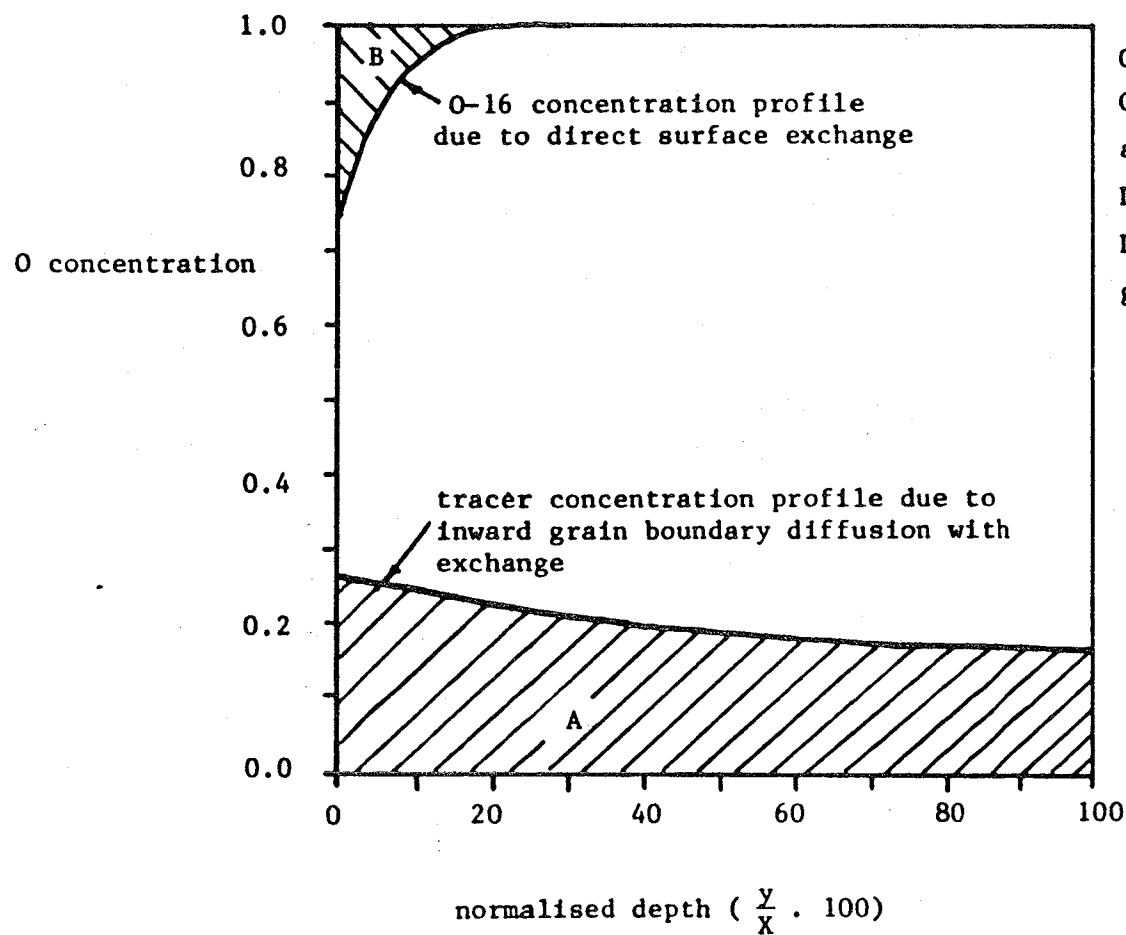
APPENDIX B

Justification of Assumptions Made

While developing the mass balance ideas in Section 3.3, it is assumed that the amount of O-16 in the old scale involved in direct surface exchange with the tracer when the sample is oxidized in O-18 gas is neglisible. The diffusion of O-16 atoms from the scale to the gas is due to the concentration gradient only and can be evaluated by setting the chemical potential gradient equal to zero. Area A in Figure 31 represents the amount of tracer retained in the old oxide due to inward grain boundary diffusion of tracer with exchange. Area B is the amount of O-16 in the old scale which undergoes direct surface exchange with a same amount of O-18 in the gas during the tracer oxidation. Area B is about 7% of area A. So the amount of tracer diffusing into the oxide due to direct surface exchange is not very significant.

O concentration

1.0

B

0-16 concentration profile
due to direct surface exchange

0.8

0.6

0.4

tracer concentration profile due to
inward grain boundary diffusion with
exchange

0.2

A

0.0

0   20   40   60   80   100

normalised depth ($\frac{y}{X}$. 100)

0-16 oxidation time-18hours

0-18 oxidation time-14hours

at $1100^{o}C$

D_b = $1.3 \times 10^{-16} m^2$/sec

D = $10^{-20} m^2$/sec

grain size = 0.3 microns

FIGURE 31 - Comparison of direct surface exchange to total exchange.

The problem of tracer exchange between the grain boundaries and grains was solved by treating the grains as spherical sinks with a constant surface concentration ϕ_y (Section 3.5). This was done for mathematical convinience so that ϕ_y could be evaluated in Equation 3.8. However ϕ_y is not a constant but is a function of time. However the assumption of a constant grain surface tracer concentration is not very severe. As shown in Figure 32, the relatively high value of grain boundary diffusivity causes the grain surface tracer concentration to rapidly reach a near steady state value. There is only about an 8% variation in the grain surface tracer concentration when the grains are being filled with tracer due to exchange. Thus the assumption of a constant does not lead to a large error.
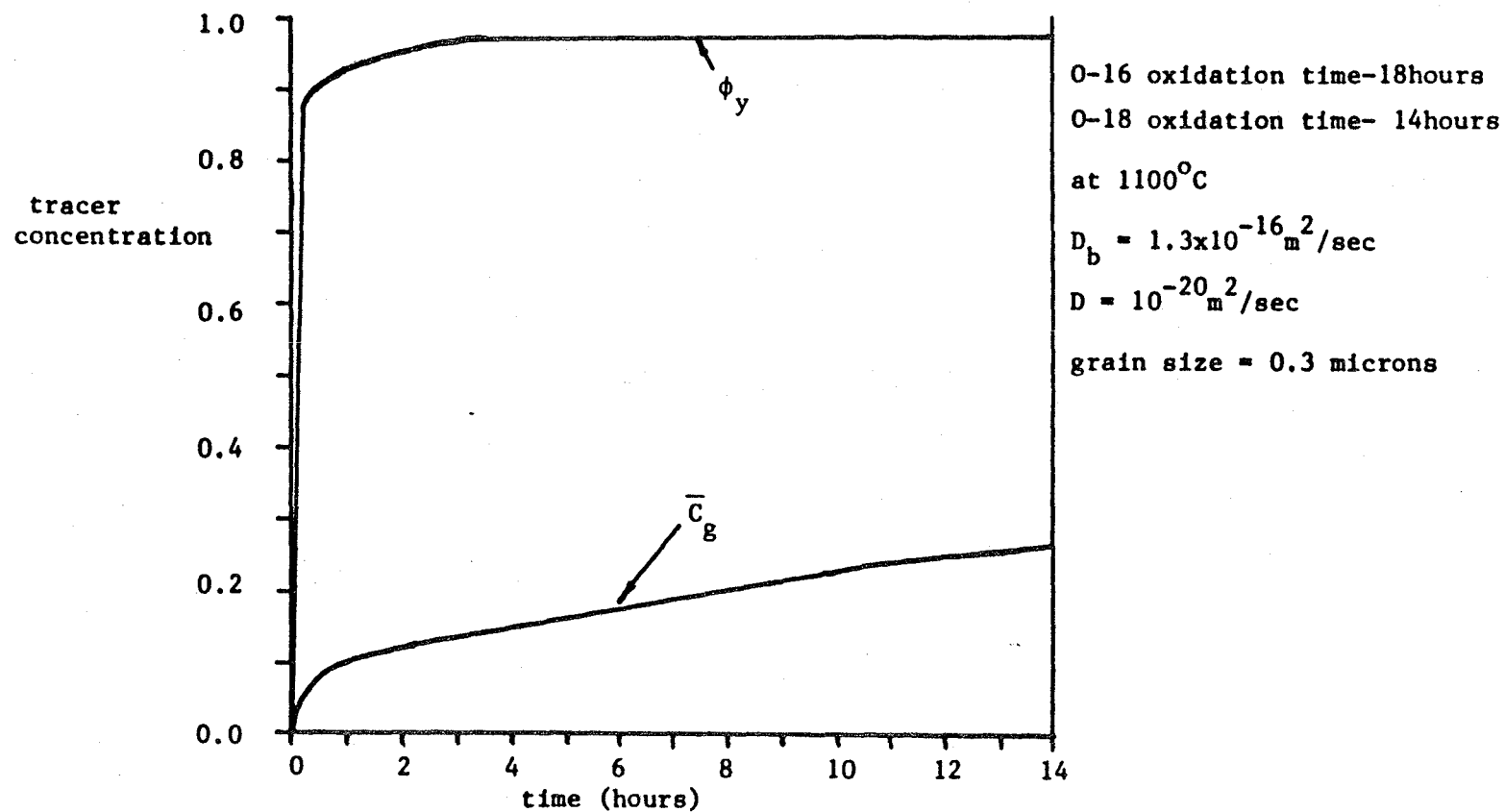
FIGURE 32 - The variation of grain surface and average grain concentration with time.

122

1. Report No.	2. Government Accession No.	3. Recipient's Catalog No.
NASA CR-174796		

4. Title and Subtitle	5. Report Date
Analysis Techniques for Tracer Studies of Oxidation	November 1984
	6. Performing Organization Code

7. Author(s)	8. Performing Organization Report No.
Soumendra Nath Basu	None
	10. Work Unit No.

9. Performing Organization Name and Address	11. Contract or Grant No.
Case Western Reserve University Dept. of Metallurgy and Materials Science Cleveland, Ohio 44106	NAG 3-324
	13. Type of Report and Period Covered

12. Sponsoring Agency Name and Address	Contractor Report
National Aeronautics and Space Administration Washington, D.C. 20546	14. Sponsoring Agency Code
	505-33-1A

15. Supplementary Notes

16. Abstract

Analysis techniques to obtain quantitative diffusion data from tracer concentration profiles were developed. Mass balance ideas were applied to determine the mechanism of oxide growth and to separate the fraction of inward and outward growth of oxide scales. The process of inward oxygen diffusion with exchange was theoretically modelled and the effect of lattice diffusivity, grain boundary diffusivity and grain size on the tracer concentration profile was studied. The development of the tracer concentration profile in a growing oxide scale was simulated. The double oxidation technique was applied to a FeCrAl-Zr alloy using O-18 as a tracer. SIMS was used to obtain the tracer concentration profile. The formation of lacey oxide on the alloy was discussed. Careful consideration was given to the quality of data required to obtain quantitative information.

17. Key Words (Suggested by Author(s))	18. Distribution Statement
O-18 tracer diffusion; Al_2O_3 scales; Oxidation	Unclassified - unlimited STAR Category 27

19. Security Classif. (of this report)	20. Security Classif. (of this page)	21. No. of pages	22. Price*
Unclassified	Unclassified	126	A07